THE SURFACE ORGANOMETALLIC CHEMISTRY OF Pd ELECTRODES: STUDIES WITH AROMATIC COMPOUNDS

A Dissertation

by

JUAN CRUZ JR.

Submitted to the Office of Graduate Studies of
Texas A&M University
in partial fulfillment of the requirements for the degree of

DOCTOR OF PHILOSOPHY

August 2012

Major Subject: Chemistry

The Surface Organometallic Chemistry of Pd Electrodes:
Studies with Aromatic Compounds

THE SURFACE ORGANOMETALLIC CHEMISTRY OF Pd ELECTRODES: STUDIES WITH AROMATIC COMPOUNDS

A Dissertation

by

JUAN CRUZ JR.

Submitted to the Office of Graduate Studies of
Texas A&M University
in partial fulfillment of the requirements for the degree of

DOCTOR OF PHILOSOPHY

Approved by:

Chair of Committee,	Manuel P. Soriaga
Committee Members,	Gyula Vigh
	Christian Hilty
	Jose Silva-Martinez
Head of Department,	David H. Russell

August 2012

Major Subject: Chemistry

ABSTRACT

The Surface Organometallic Chemistry of Pd Electrodes:

Studies with Aromatic Compounds. (August 2012)

Juan Cruz Jr., B.S., University of Texas at El Paso;

M.S., University of Texas at San Antonio

Chair of Advisory Committee: Dr. Manuel P. Soriaga

To help establish the surface coordination and organometallic chemistry of palladium electrodes, the chemisorption properties (coverage, orientation, and reactivity) of selected aromatic compounds in aqueous solutions were investigated. Thin-layer electrochemistry was employed with atomically smooth polycrystalline electrodes to extract information on surface packing densities and adsorbate cross sections. Comparison of the latter with calculated values allowed the determination of the more plausible adsorbed-molecule orientations; in a few cases, verification was obtained via surface vibrational (high-resolution electron-energy loss) spectroscopy. Eleven aromatic compounds were studied: [hydroquinone (1), benzoquinone (2), methylhydroquinone (3), 2,3-dimethylhydroquione (4), 2,3,5-trimethylhydroquinone (5), 1,4-dihydroxynaphthalene (6), phenylhydroquinone (7), 2,3-dihydroxypyridine (8), 2,5-dihydroxythiophenol (9), 2-(8-mercaptooctyl)-1,4-benzenediol (10), and hydroquinone sulfonic acid (11)]. For the homoaromatic compounds, chemisorption was oxidative to form surface-coordinated quinones; flat orientations were observed at low

concentrations, vertical orientations at much higher concentrations. The presence of substituents more surface-active than the aromatic moiety induced other orientations. Preferential chemisorption was found to increase in the order: phenyl ring < quinone ring < -SH.

DEDICATION

To my mother, Carmen Ramirez Cruz

ACKNOWLEDGMENTS

I wish to thank my research advisor, Dr. Manuel P. Soriaga, for his patience and guidance. I also thank my committee members, Dr. Gyula Vigh, Dr. Christian Hilty, and Dr. Jose Silva-Martinez for their valuable guidance and comments on my dissertation.

I would like to thank all former and current members of Dr. Soriaga's research group for their academic advice and friendship. Most of all, I would like to thank Dr. Jack H. Baricuatro for his mentoring, encouragement, and friendship during the early part of my graduate education. I would also like to thank Kyle Cummins and Alnald Javier for their help, advice, and friendship.

I would like to acknowledge support of this work by the Department of Chemistry and the Robert A. Welch Foundation. Special thanks are due to The Veterans Administration Education Benefits whose financial support was indispensable. I am grateful to the U. S. Air Force Reserves and 26th Aerial Portals Squadron for the education benefits through the years.

I would like to thank my friends and colleagues and the department faculty and staff for making my time at Texas A&M University a great experience. I am also especially thankful to Sandy Manning, Bill Merka, and Julie A. Zercher.

I acknowledge my mother, brothers, wife, son, daughter, nephew, niece, and sister-in-law for their unwavering love and support for my education.

TABLE OF CONTENTS

LIST OF FIGURES

LIST OF TABLES

1. INTRODUCTION

Palladium (Pd) is widely used as a heterogeneous catalyst for the selective hydrogenation of olefins [1-4]. In the hydrogenation of an aromatic ring, the reaction is greatly increased when Pd is combined with a tethered rhodium isocyanide complex, $RhCl[CN(CH_2)_3Si(OC_2H_5)_3]_3$ [5]. Pd is also used for carbon-carbon coupling, oxidation of benzylic and allylic alcohols, and hydroalkylation [6-8]. These selective reactions can be attributed to Pd properties. Compared to its congeners, Pd is unique since its physicochemical attributes do not follow the typical trend down a group in the periodic table. For instance, ΔH^0_{diss} of Pd_2 is only 100 kJ/mol compared to 203 kJ/mol of Ni_2 and 357 kJ/mol of Pt_2. Similarly, the enthalpy of atomization (cohesive energy) of Pd is 376 kJ/mol—a value much smaller than that of Ni (428 kJ/mol) or Pt (564 kJ/mol). The low enthalpy energies of Pd indicate a weak intermetallic Pd-Pd bond. This property also suggests lateral mobility of Pd surface atoms.

The heterogeneous Pd catalyst is used for many hydrocarbon reactions such as hydrogenation, dehydrogenation, hydrogenolysis, isomerization, and dehydrocyclization. It is also used in the initial step of the oxidation of ammonia for fertilizer production [9]. In order to better utilize Pd as heterogeneous catalysis it is necessary to explore the surface catalytic process.

This dissertation follows the style of the Journal of Electroanalytical Chemistry.

Surface coordination chemistry between transition metals and organic ligands has drawn great attention because understanding the chemistry at the metal surface is key to designing or enhancing catalytic reactions. While ultrahigh vacuum (UHV) studies of the gas-solid interface have provided valuable information about adsorbate-substrate interactions, these studies are conducted in the absence of an electrochemical environment. Pt is one of the few metal with significant studies in correlating the interaction between gas-solid and solution-solid interface [10-16], yet investigations on surface structures of organic molecules and their surface confined electrochemical reactions on Pd surfaces remain sparse [4,16-18].

Surface analytical instruments have helped to increase our knowledge of the heterogeneous reactant-metal (adsorbate-substrate) interactions. Since surface activity is dependent on the surface structure, low-energy electron diffraction (LEED) is widely used to determine the type of surface structures, such as a (110), (100), and (111) [1,19,20]. This technique can also be used to determine the adsorbate structures. Reflection-adsorption infrared spectroscopy (RAIRS), and high-resolution electron energy loss spectroscopy (HEERLS), can be employed to study the adsorption sites and geometries between the adsorbate and surface [1,19,20]. Thin-layer electrochemistry (TLE) is another technique used to study the interaction between the adsorbate and metal surface [21-23]. However, the TLE method is much simpler because results are readily obtained by measuring the charge from the electroactive in the species thin-layer solution. TLE is limited in determining the types of bond formation between the

adsorbate and surface. Therefore, the utilization of both TLE and a surface analytical technique can greatly increase knowledge of the liquid-solid interface.

1.1 Chemisorption and physisorption

As the atom or molecule approaches the surface, three outcomes are possible. One outcome is bouncing off the surface by the atom/molecule. The other two outcomes are the interaction between the atom/molecule and interaction with the surface. The first interaction is the physical adsorption (physisorption) of the molecule to the surface without bond formation. Physisorption is the balance between weak attractive forces (e.g. Van der Waals) and repulsive forces (e.g. electron–electron). The adsorbed atom, or molecule, is called the adsorbate, and the adsorbing surface is called either the adsorbent or the substrate. The heat of adsorption, ΔH_{ads}, is always exothermic with values ranging from -10 to -40 kJ/mol. Physisorbed species are not bound to any specific surfaces site, such as (111), (100), and (110) [1,20]. Instead, the adsorbate interacts uniformly across the surface. The weak interaction of adsorbate-substrate allows a stronger adsorbate-adsorbate interaction, and the adsorbate readily forms ordered structures. Therefore, the surface physisorption state is the major factor in determining the extent in surface density of adsorbate before chemisorption. However, other adsorbates (e.g., sulfur) are directly chemisorbed while bypassing the physisorption well [1,2,19].

In chemisorption, the exchange of electrons between the adsorbate and substrate

forms a chemical bond. This chemical interaction is called chemisorption. Unlike physisorption, chemisorption is highly directional to specific surface sites (e. g. bridging) and favors high coordination numbers. The bond strength of the adsorbate-substrate depends on the crystallographic structure of the surface. In the study of Rh, Pt, and Pd electrodes, the trend for the surface activity was (111) > (100) > (110), respectively [1,2,20,24]. The chemisorption process has two types of surface chemical reactions. A non-dissociative chemisorption is a bond formation between the adsorbed molecule and the surface, while the overall interatomic bonds of the molecule remain intact. This chemisorption can be represented by the Equation 1:

$$AB \rightarrow AB_{ads} \quad (1)$$

Figure 1 shows the potential curve for the physisorption and chemisorption states. The physisorption energy curve is an approximation by the Lennard-Jones (9-3) potential and described by Equation 2:

$$V(z) = 4\pi\varepsilon N_s\sigma^3[45^{-1}(\sigma/z)^9 - 6^{-1}(\sigma/z)^3] \quad (2)$$

where the z is the distance between the adsorbing molecule and surface, ε is the chemisorption well (heat of adsorption, ΔH_{ads}), N_s is the number of moles of the surface atoms, and σ is the interatomic distance at which the potential energy crosses zero [1]. The variable $1/z^9$ represents the repulsive interaction of the molecule-atoms, while the

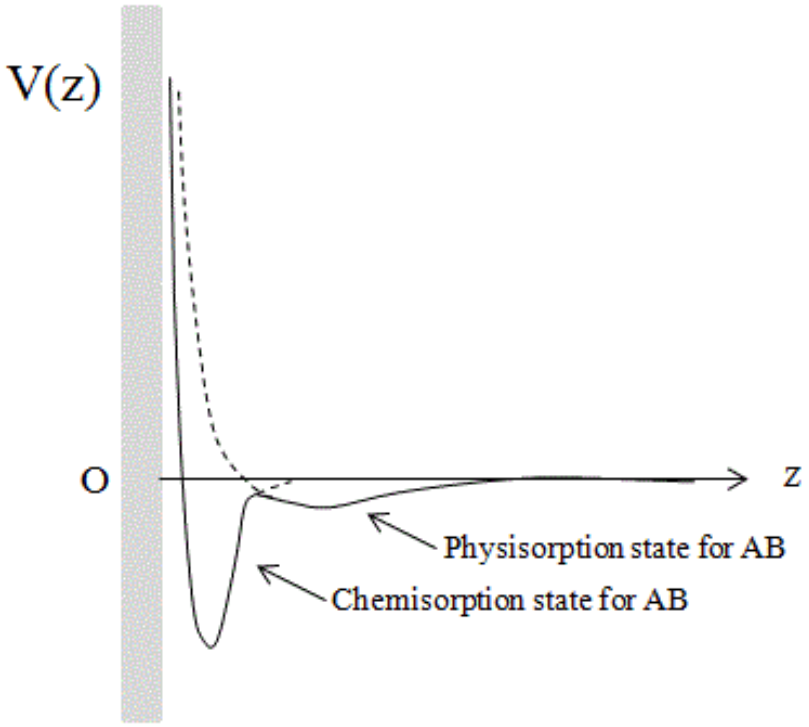

Figure 1. The non-dissociative chemisorption potential energy curve. The physisorption state is shown by a dashed curve and lowest energy pathway is shown as a solid line [1].

$1/z^3$ is the attractive interaction between the molecule and surface atoms. The chemisorption energy curve is an approximation by the Lennard-Jones (12-6) potential, and described by Equation 3:

$$V(r) = 4\varepsilon[(\sigma/r)^{12} - (\sigma/r)^6] \quad (3)$$

where r is the interatomic distance, ε is the chemisorption well (heat of adsorption, ΔH_{ads}), and σ is the interatomic distance at which the potential energy crosses zero [1]. As the distance decreases between the molecule and surface, the molecule is momentarily trapped in the physisorption well until it overcomes the energy barrier (energy of activation, E_a). At this point, the molecule becomes trapped in the chemisorption well. Table 1 summarizes the chemical and physical trends of chemisorption and physisorption [1,2,25]. The physisorption and chemisorption processes have been widely studied, with the help of CO, on several metal surfaces [1,2,19]. The interaction between CO and the metal atoms is a synergic bond. This type of bonding is also present in CO and the metal surface. A synergic bond is the combination of a σ and π bond between the CO and the metal atom. The non-bonding electrons from 5σ orbital (highest occupied molecular orbital, HOMO) localized on the carbon atom form a weak bond with the d-orbital of the metal atom as shown in Figure 2a. This CO-metal (such as Rh, Ni, Pd, Pt, and other transition metals) bond has been confirmed by several experimental data and theoretical calculations. In addition, the electron density of the d- orbital (metal atom) are transferred to the empty the π^*

Table 1. Summary of Chemisorption and Physisorption Properties [1,19,25].

Physisorption	Chemisorption
polarization	electron exchange
van der Waals attractions	chemical bond formation
$\Delta H_{(ads)}$;	$\Delta H_{(ads)}$;
(-10 to 40 kJ/mol)	(-146 to 272 kJ/mol)
monolayer and multilayers	monolayer

orbital (lowest unoccupied molecular orbital) of CO as showed in Figure 2b. The amount of back bonding from the d-electrons to the π* orbital of CO depends on the transition metals.

The electron donation also depends on the level of Fermi energy (E_f) in comparison to the energy of the π* orbital. Transition metals on the right side of the periodic table have lower E_f than the π* orbital, so the back bonding is minimal [1,19]. Since the back bonding does not occur on the π* orbital of the CO, the bond between CO remains strong. On the left side of the periodic table, the transition metals have higher E_f than π* orbital. Consequently, the back bonding readily occurs and weakens the CO bonds while stabilizing the CO-M bond [26,27]. The amount of back bonding to the empty π* orbital determines whether the dissociation or non-dissociation of the chemisorbed CO occurs. This synergic bonding is analogous to the CO bonding to surface metals such as Rh, Ni, Pd, and Pt. Figure 2c shows the interaction between CO and a metal surface.

1.2 Analogy between heterogeneous and homogeneous systems

Figure 3 shows a schematic of three surface coordination chemical systems, which are similar to their homogenous coordination counterparts. In all the reactions, the adsorbate, or ligand, formed a bond with the metal. In the surface-immobilized complex,

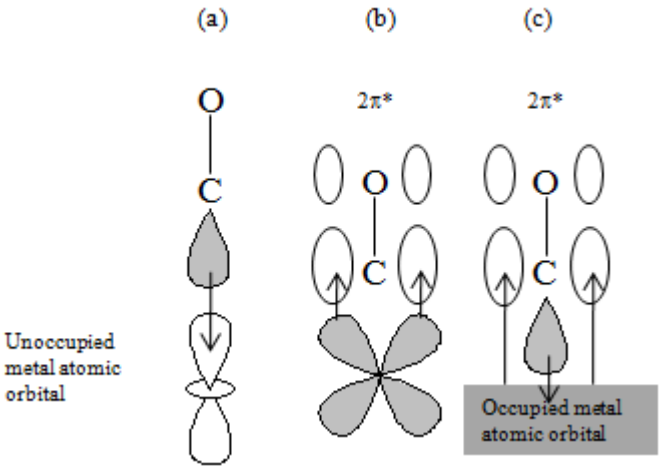

Figure 2. A schematic diagram of synegic bonding of CO to a metal. The interaction of (a) the 5σ orbital and (b) the 2π* orbital with a metal in a metal carbonyl compound. (c) The interaction of adsorbed CO with the surface [1].

the metal complex is tethered to the metal surface. The active site of the anchor complex becomes positioned in the solution phase instead of the surface. This location allows the active site to have similar reactions as the homogenous coordination chemistry. Since we are interested in the interaction between the surface and ligand, the surface-immobilized complex is not a concern in this research.

The third system has similarities to homogenous coordination chemistry. In an electrochemical system, the surface is mostly covered with weakly coordinating electrolyte (e.g. SO^{4-}) and solvent molecules (e.g. H_2O) [28-30]. This adsorbed species (ligands) can be easily displace from the surface a by a ligand with higher surface affinity [25,31]:

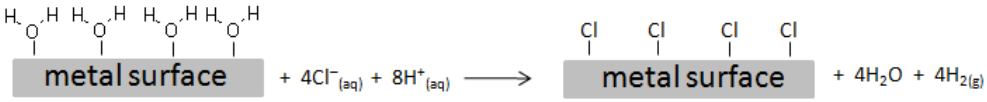

(4)

In the heterogeneous coordination chemistry, the Cl^- is oxidized to Cl^0 while H^+ is reduced to H_2 gas. This surface reaction allows the metal surface, like Pt and Pd, to maintain a zero valent oxidation state unlike the homogeneous coordination reaction. The surface-ligand reaction is similar to the homogeneous coordination reaction in which a stronger ligand displaces a ligand bound to a central metal except the oxidation state of the metal [16,26,27]. For example, $Ni(OH_2)_4^{2+}{}_{(aq)} + 4Cl^-_{(aq)} \rightarrow NiCl_4^{2-}{}_{(aq)} + 4H_2O$. In the above example, the Cl^- ligands maintain the oxidation state (-1) after forming a bond with nickel cation, but the oxidation state of the nickel changes from 2^+ to 4^+. The

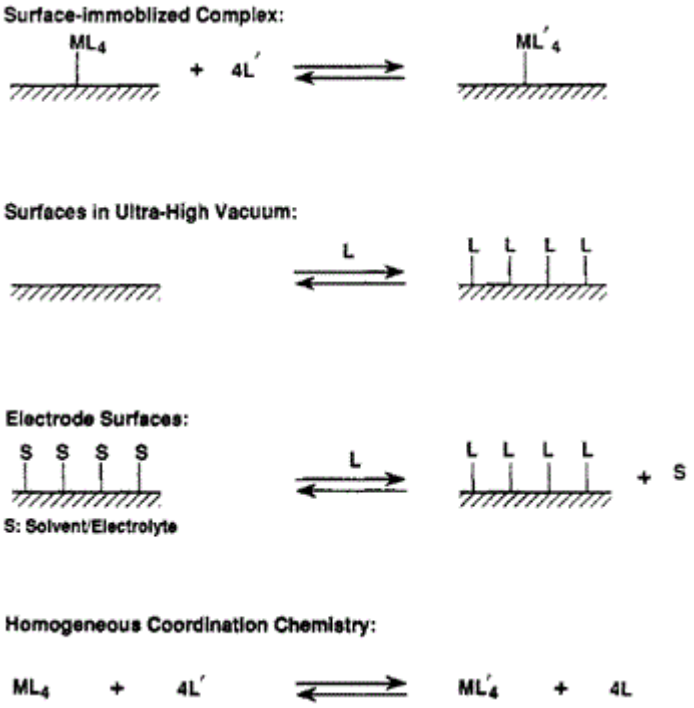

Figure 3. Schematic of the similarities and differences between surface heterogeneous systems and homogeneous coordination chemistry [32] .

oxidation or reduction of the central metal atom or ion readily occurs in homogenous coordination chemistry. In an oxidative addition reaction, the addition of a nonmetal species (e.g. Cl_2, CH_3I, or HCl) can increase the oxidation number of the center atom or ion. One example is tetracholoropalladium(II) reacting with chlorine gas to form hexachloropalladium(IV) shown in Equation 5:

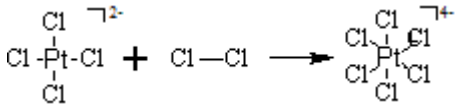

(5)

In the reduction of the metal, two species leave the metal complex which results in a decrease in the oxidation number.

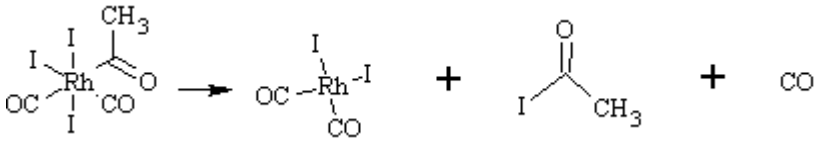

(6)

In a heterogeneous system, the applied positive potential on the metal surface does not form cations, instead it forms an oxide film on the surface [24]. The onset of surface oxidation varies with different metal electrodes. For example, the oxidations for Rh, Pd, Pt, and Au start at 0.31 V, 0.48 V, 0.55 V, and 1.0 V, respectively. At higher potentials, Pd, Rh, Pt, and Au electrodes produce $O_{2(g)}$ from the water oxidation instead of metal cations. At negative potentials, the surface metal atoms are not reduced, instead the atoms reduce water to atomic hydrogen within the bulk. In Pd, Pt, Au, Pt, and Rh

hydrogen evolutions occur at 0.0 V, 0.15 V, 0.22 V, and -0.15 V, respectively. Pd has a tendency to adsorb large amounts of hydrogen atoms into the bulk of the metal. In order to maintain a zero-valent state of the metal surface for the study of heterogeneous coordination chemistry, the applied potential of the electrode must be lower than the onset of the metal oxide films. This potential range is called the double layer region. Even with the different chemical characteristics, homogenous coordination chemistry can be used to better understand the heterogeneous coordination chemistry.

1.2.1 Chemisorption vs. synthesis

The analogies between heterogeneous and homogeneous coordination chemistry are presented on Table 2. In the heterogeneous systems, the solvent also functions as ligands as in the homogeneous coordination chemistry. The CO ligand in both systems forms a bond with the electrode surface or central metal [1,19,27]:

$$Pd_{(s)} + CO_{(aq)} \rightarrow Pd - CO_{(ads)} \quad (7)$$

$$Pd_{(g)} + 4CO_{(g)} \rightarrow [Pd(CO)_4]_{(g)} \quad (8)$$

These reactions are called chemisorption (1) for surface coordination chemistry, and synthesis (2) for homogeneous coordination chemistry. In addition, many other molecules, such as aromatic compounds, are readily chemisorbed on the metal surface [33-39].

Table 2. Comparison between heterogeneous and homogenous coordination chemistry [32].

electrode surface	molecular/cluster complex
chemisorption	synthesis
adsorbate orientation	mode of coordination
competitive chemisorption	ligand of substitution
adsorbate exchange	ligand exchange
adsorbate reactivity	ligand reactivity
electrocatalysis	homogenous catalysis

1.2.2 Adsorbate orientation vs. mode of coordination

Adsorbate orientation is similar to the mode of coordination, because both systems require a ligand with different potential donor atoms [26,27]. This type of ligand is called an ambidentate. For example, thiocyanate ions (NCS^-) can attach to the metal atom at the nitrogen atoms (M-NCS) to produce isothiocyanato complexes, or attach at the sulfur atom (M-SCN) to produce thiocyanato complexes. Similarly, hydroquinone has two different potential donor atoms. Hydroquinone can attach from the π-bonds or C-H bond. In the homogeneous chemistry, the π-bonds of benzoquione form a η^6 bond with Pt to create (benzoquinone)bis(triphenylphosphine)platinum(II). In a metal cluster, the η^2 bond occurs from two intermolecular C-H cleavage reactions to form a di-σ-bonde hydroquinone. Both orientations can be summarized in the following [40]:

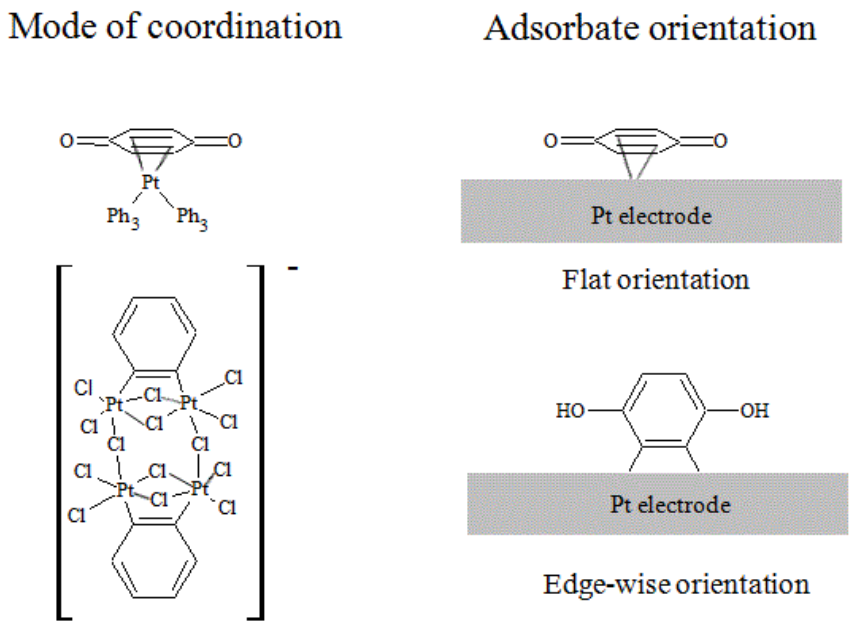

(9)

The activation of the C-H bonds is not limited to Pt and Pd. Many other transition metals, such as Ru, Rh, and Ir also activate the cleavage of C-H. Therefore, adsorbate orientation is dependent on the atoms involved in the interaction with the surface**.**

1.2.3 Competitive chemisorption vs. ligand substitution

In the ligand substitution for homogeneous chemistry, an incoming ligand displaces a ligand from the central metal atom. The entering group can displace all the ligands from the metal atom when the formation constant (β) of metal complex is large than the bound ligand to the central atom[27]. A large β indicates a ligand with a strong binding energy with the central atom, versus a weak binding energy for a small β. In Pd complex with halogens, a chloro ligand is easily displaced by a bromide ion, and a bromo ligand is displaced by an iodo ligand [32]. Therefore, the strength of the ligand increases in this order: Cl^- < Br^- < I^-. This trend is also followed in the formation constant [1.6×10^6 (Cl^-) < 1.3×10^{16} (Br^-) < 7.9×10^{24} (I^-)]. In the heterogeneous coordination chemistry, the trend for the chemisorption of the halides on Pd surface was the same as the ligand substitution in homogenous coordination chemistry [25]. The bromide ions displace the Cl^0 from the Pd surface while Br^0 gets displace by iodide ions. The chemisorbed I^0 remains on the surface in the presence of chloride ions. The halides follow the same trend during the competitive chemisorption on Pt surface. These experimental results were compared to the temperature programmed desorption experiments. The ΔH_{ads} increases in the order of 35 kcal (Cl^-) < 50 kcal (Br^-) < 65 kcal

(I^-), which is identical to the formation constant [25]. The heterogeneous and homogeneous reaction for the competitive chemisorption vs. ligand substitution is illustrated by the following equations:

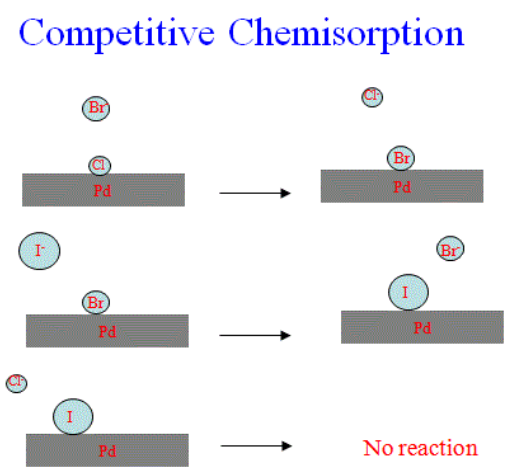

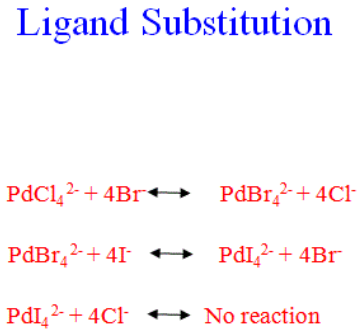

ΔH(ads) kcal/mol	
Cl	35
Br	50
I	65

Formation constant, β	
Cl^-	1.6×10^{12}
Br^-	1.3×10^{16}
I^-	7.9×10^{24}

(10)

1.2.4 Adsorbate exchange vs. ligand exchange

Adsorbate exchange parallels the ligand exchange in which a stronger ligand displaces a weaker ligand from central atom. The strength of the ligand depends on the ability of the atom to donate a lone electron pair to an electron-poor metal atom. For example, the ligand order for Pt(II), Pt(II), and Ir(II) is found in Equation 10 [26,27]:

$$H_2O < Cl^- < I^- < H^- < PR_3 < CO, CN^- \quad (11)$$

A stronger ligand tends to form a stronger bond with the central metal atoms. For this reason, good nucleophiles (ligands) are harder to displace from the central atom by weak nucleophiles. In surface coordination chemistry, the ligands exhibit the same order during the chemisorption on Pt surface. The analogy between the homogenous and heterogeneous can be described by the following reactions [26,32]:

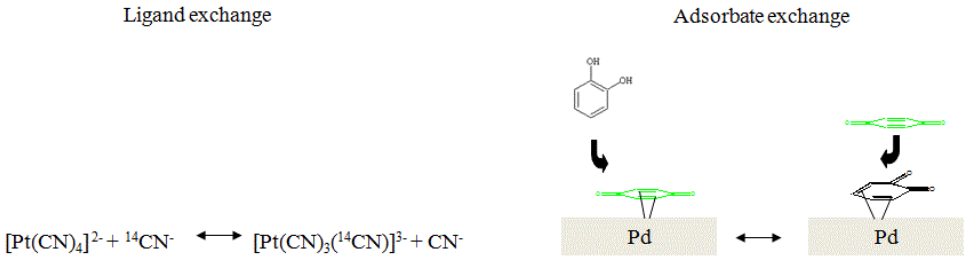

(12)

1.2.5 Adsorbate reactivity vs.ligand reactivity

A comparison of cyclic voltammogram between adsorbed and un-adsorbed 2,5-dihydroxythiophenol (DHT) shows that both have reversible redox peaks with similar potentials. This result confirmed the electroactivity of the diphenol group of DHT. However, the voltammetric curve of Pt was broader than the voltammetric curve of DHT on the Au surface, even when both surface coverages are very similar (Pt: of 0.56 +/- 0.04 nmol cm^2 and0.54 nmol cm^2) [41,42]. These values are also similar to the calculated 0.57 nmol cm^2 for DHT with a vertical S-η^1. As a result, the peak broadening can be attributed to possible adsorbate-adsorbate interactions. If the interaction occurred through space from the pendant DHT, both voltammetric curves would be identical, as

both surface coverages are similar. Therefore, a quinone/diphenol couple is only possible through the metal surface (substrate-mediated). The interaction might produce the presence of a quinhydrone complex, which is known to be highly stable in a 1:1 quinone to diphenol ratio within the adsorbed DHT. The quinone/diphenol couple is illustrated as follows [32]:

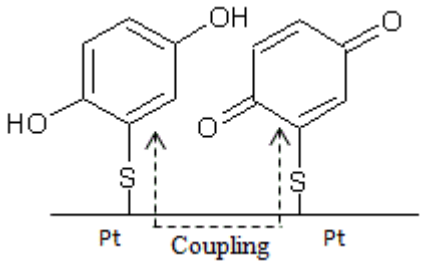

(13)

The substrate-mediated coupling is not limited to a metal surface. Bidentate ligands, such as pyrazinyl, 4,4'-bipyridyl (bpy), 3,3'-dimethyl-4,4'-bipyridylmethane, and 4,4'-bipyridylamine [43,44], can also function as a bidentate ligand-mediated coupling for a binuclear pentaammineruthenium:

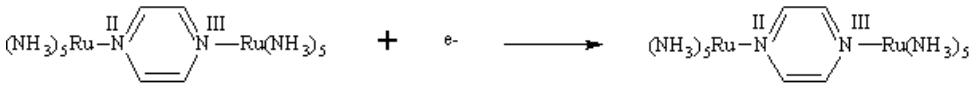

(14)

In this system, the bipyridylamine ligand with a delocalized electron, allows the Ru atoms to interact for a redox reaction. The Pd electrode also provides a venue for charge-transfer between two DHT molecules. Figure 4 shows the cyclic voltammogram of chemisorbed DHT on a Pd electrode. In the cathodic scan, the peak is broader than the

anodic peak. This type of CV also occurs while using a Pt electrode [45]. However, the use of an Au electrode results in the absence of the broadening of the redox peaks for chemisorbed DHT. Therefore, the quinone/diphenol couple is only possible through the metal surface (substrate-mediated), instead of the adsorbate-adsorbate interaction through space between the pendent hydroquinone moieties.

1.2.6 Electrocatalysis vs. homogeneous catalysis

The electrocatalytic hydrogenation reaction is also dependent on the surface orientation of the adsorbed organic. The surface reactivity can be illustrated by the following reaction:

$$\text{organic}_{(ads)} + n_H H^+ + n_H e^- \rightarrow \text{hydrogenation product} \quad (15)$$

Where n is the number of electrons transferred during hydrogenation desorption [46-48]. TLE was utilized to measure the amount of reduction for the chemisorbed organic and the adsorbed hydrogen on the bare metal electrode. The hydrogenation of the organic was determined for the flat and edgewise orientation. The experimental results revealed several surface activities [49]. Hydrogenation is dependent on adsorbed hydrogen, and the reduction rate increases with higher negative potential. However, the reduction is limited to a portion of the chemisorbed organic. The desorbed aromatic ring is completely reduced to cyclohexane. By comparing the experimental and calculated

ratios of the moles of adsorbed hydrogen (n_H), and the loss of the organic in solution (n_H), the experimental ratio of 6.4 was very similar to the calculated ratio of 6.0 for the 1,4-cyclohexanediol. GC/MS analysis of the solution confirmed the presence of 1,4-cyclohexanediol from the reduction of η^6-BQ at -0.13 V. At a higher negative potential (-0.25 V), the experimental ratio remains constant because the higher desorption of BQ is proportional to higher adsorption of hydrogen [50]. The hydrogenation of 2-3-η^2-H2Q is similar to that of η^6-BQ in which the carbons bonded to the surface are reduced. The ratio for 2-3-η^2-H2Q reduction, however, is not similar to that of cyclohexane-3,5-diol. 2-3-η^2-H2Q has a ratio of 10 compared to the ratio of 6 for the cyclohexane-3,5-diol.

The anodic oxidation of chemisorbed H_2Q/BQ is dependent on the molecular orientation. The adsorbate oxidation can be described by the following equation:

$$\text{organic}_{(ads)} \rightarrow \text{oxidation product} + n_{ox}e- \quad (16)$$

Where n_{ox} is the number of electrons transferred to oxidize and desorb an adsorbed molecule. The TLE technique was used to determine the orientation of H_2Q/BQ on the surface of the Pd electrode. The oxidation of η^6-BQ resulted in an n_{ox} of 22.2 +/-0.3 compare to the n_{ox} of 24 for the complete oxidation of carbons from the aromatic ring as shown in Equation 16:

$$\eta^6\text{-}C_6H_4O_2 + 10H_2O \rightarrow 6CO_2 + 24H^+ + 24e- \quad (17)$$

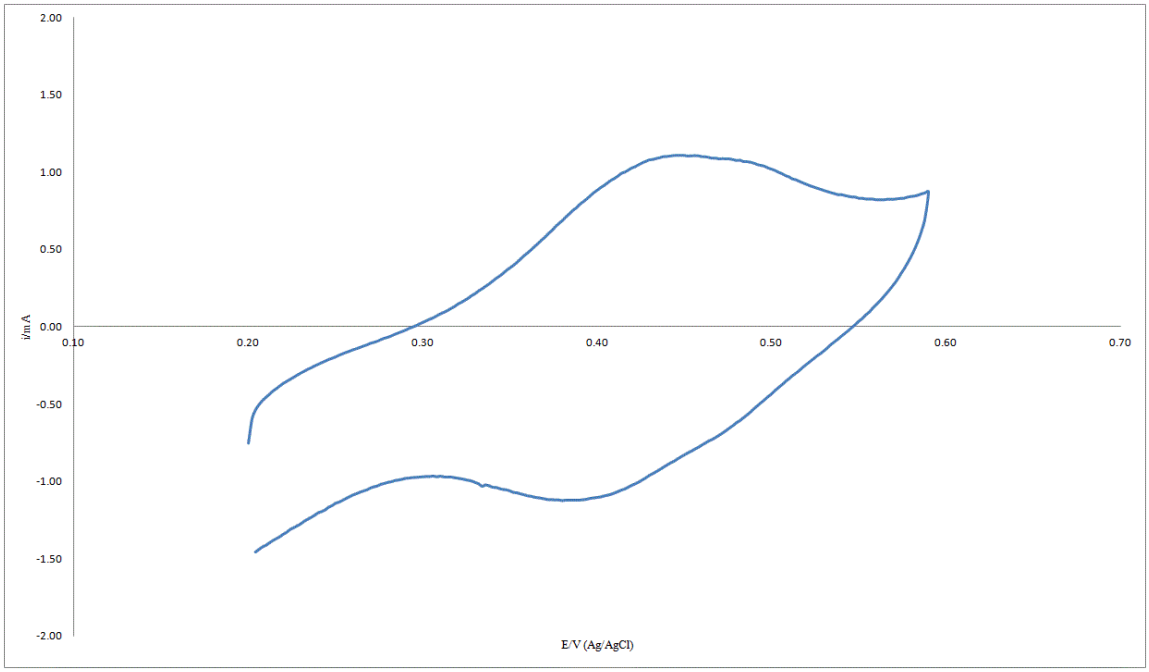

Figure 4. Cyclic voltammogram of DHT after exposing the Pd electrode to 1.0 mM DHT solution of 1.0 M H_2SO_4 for 180 seconds. Scan rate, 2 mV/s.

The oxidation of 2-3-η^2-H_2Q has a value of 15, which is smaller than the value for the η^6-BQ [46]. This difference indicates the electrocatalytic oxidation is also dependent on the molecular orientation as in the electrocatalytic hydrogenation. The n_{ox} of 15 is similar to the oxidation product of maleic acid (n_{ox} = 12) and tartaric acid (n_{ox} = 14):

$$\eta^2\text{-}C_6H_4O_2 + 6H_2O \rightarrow 2CO_2 + C_4H_4O_4 + 12H^+ + 12e\text{-} \quad (18)$$

$$\eta^2\text{-}C_6H_4O_2 + 8H_2O \rightarrow 2CO_2 + C_4H_6O_6 + 14H^+ + 14e\text{-} \quad (19)$$

The two completely oxidized carbons are the C_2 and C_3, because these carbons are the only ones directly chemisorbed to the surface. The other four carbons have minimum oxidation. It is possible that maleic acid is the actual product, as it was present in the oxidation of η^2-$C_6H_4O_2$ on the Pt electrode [51]. In all the above experimental results, the electrocatalytic hydrogenation and oxidation of adsorbed organics are dependent on the mode of surface coordination.

1.3 Objective

The objective of this research was to study the effect of concentration on the mode of chemisorption of aromatic compounds on a Pd electrode surfaces to help establish the surface organometallic chemistry of Pd.

2. EXPERIMENTAL

2.1 Thin-layer electrochemistry (TLE)

Thin layer electrochemistry allows for oxidation-reduction reactions to occur in a confined space between the cell wall and electrode (2-100 μm) [23]. The thin layer (TL) cavity design provides advantages comparable to conventional electrochemistry methods such as:

1 non-existing mass transportation due to the smaller cell thickness compared to the diffusion layer thickness

2 surface contamination minimization due to the small volume (e.g. μL)

3 isolation of product species from surface reactions

4 high surface to volume ratio increase to the electroactivity of surface reactions relative to solute reactions

In the study of surface adsorption by organic species, the sensitivity of TLE allows the measurement of surface coverage at the nmol/cm^2 range. It is also used to determine the surface coverage (r = nmol/cm^2) and molecular orientation on a clean polycrystalline Pd surface.

Figure 5 shows the thin-layer electrochemistry cell. The polycrystalline Pd is of cylindrical shape and is located inside the glass cavity [48]. The diameter of the Pd is slightly smaller than the diameter of the cavity, resulting in a small gap between the Pd and the glass. The filling of the cavity with solution occurs from capillary action through

the pin holes at the bottom of the cavity. The Teflon stopcock is used as a valve to control the nitrogen gas passing through the thin-layer cell. The removal of solution is accomplished by passing pressurized, high-purity H_2 gas through the TLE inlet. The cavity is re-filled with fresh solution once the pressurized H_2 gas is stopped.

A stainless steel mandrel (3.12 mm and 11 mm length) is inserted into a glass tube (3.12 mm I.D. x 6.90 O.D. x 11 mm length.). The inner diameter of the glass tube is slightly larger than 3.12 mm to allow the insertion of the mandrel. A Pyrex® tubing, with a 7 mm I.D. x 9 mm O.D., is also cut to a length of 11 mm. The glass tube with the mandrel is inserted into the section of Pyrex® tubing. The whole piece is placed in a quartz tube and heated to 900 ^{0}C causing the mandrel to expand up to 0.025 mm and the fusion of the glass and Pyrex® tubes.

Since the thermal expansion of the stainless steel mandrel and Pyrex® tube are different, a small space between the mandrel and Pyrex® tube is formed when the assembly is cooled to ambient temperatures. The removal of the mandrel leaves an inner tube of precise and reproducible dimensions. This tube section is inserted at the end of the standard wall glass tube (10 mm I.D. and 15 cm length), and the glass pieces are fused together. The heating steps are carried out with extreme care to prevent any damage of the cavity. The fabrication of the two pin holes is identical to the procedure described earlier.

A cylindrical polycrystalline (pc) Pd electrode was used in this research and shown in Figure 5. The pc-Pd electrode is made from a Pd rod (99.99% purity,

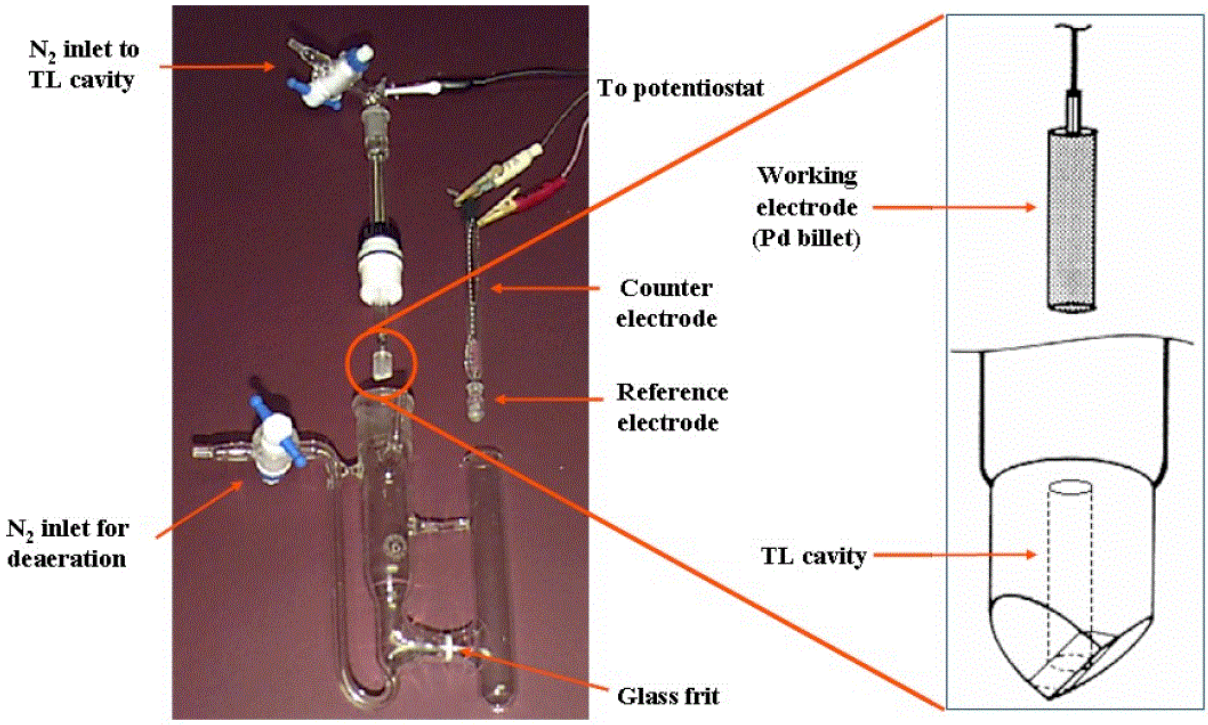

Figure 5. (a) Thin-layer electrode and H-cell set-up. (b) Close-up view of thin-layer cavity and Pd billet [17,52].

Wilkinson Co., Westlake Village, CA) with dimensions of 3.81 mm × 12.0 mm. To obtain an electrode with a diameter of 3.12 mm, the cylinder was machined with a mill to a tolerance of one-thousand of an inch. The electrode was polished with successive grades of 7.0 μm and 0.25 μm diamond paste until the surface has a near-mirror finish by a mill. In order to obtain a clean and atomically smooth surface, a pc-Pd electrode is annealed in a H_2/O_2 flame until it becomes red. The electrode is allowed to cool slowly before it is immersed in ultra pure water (Milli-Q Gradient, Fisher Scientific Co).

2.2 Solid-liquid electrochemical interfaces

At the solid-liquid interface, two solution layers of a different composition from the bulk solution are formed [23,29,53,54]. When a negative (or positive) potential is applied to an electrode, a negative (or positive) charge, q^m, accumulates on the surface. This flow of charge is called a charging current, and the thickness of the excess (or deficiency) charge, $q^{M,}$ is less than 0.1 Å. The electrolyte and other species form an opposing charge, $-q^S$, adjacent to the electrode surface. The amount of charge is dependent on the surface area, so the charge is mostly reported as charged density. The charge density, σ^M, is equal to q^m/cm^2. The $-q^S$ is composed of two solution layers: The inner layer is located on the electrode surface, and the outer layer is adjacent to the inner layer. The inner layer is a two dimensional while the outer layer is a three dimensional. This layer is known as a Helmholtz layer, as shown in Figure 6. The thickness, x_1, is measured from the locus of the electrical center of the adsorbed anion [23,29,53,54]. The

x_1 is called the inner Helmholtz plane (IHP). Solvent and other species (ion or molecules) in the IHP plane are considered specifically adsorbed. In the Figure 6, anions are specifically absorbed, because the specie and charge metal interact by electrostatic force. The specifically adsorbed species give a charge density of σ^i ($\mu C/cm^2$). The other layer is made from solvated cations near IHP. The distance, x_2, between the locus of center (cations) and the surface is called the outer Helmholtz plane. The greater the distance from the charged metal, the lower the interaction between the solvated cations and the electrostatic forces. The cations formed a non-specific orientation with respect to the charged metal**.** These cations are considered non-specifically adsorbed. The weak surface interaction allows cations to be in three-dimensional region by the presence of a thermal agitation in the solution. The region is called the diffuse layer and extends from the OHP into the bulk of the solution. The diffuse layer also has a charge density of σ^d.

$$\sigma^M = -\sigma^i + -\sigma^d = -\sigma^S \tag{20}$$

A negative potential produces a negative charge density, $-\sigma^M$, on the surface of the electrode, and an opposite charged density, σ^S, at the solution. The overall charge density, given by the thickness of the diffuse layer, is ~20 to 300 Å, and depends on the total ionic concentration in the solution. For example, for a solution with a concentration greater than 10^{-2} M, the thickness is less than ~ 100 Å [23,29,53,54].

The potential profile across the double-layer region is shown in Figure 7. The

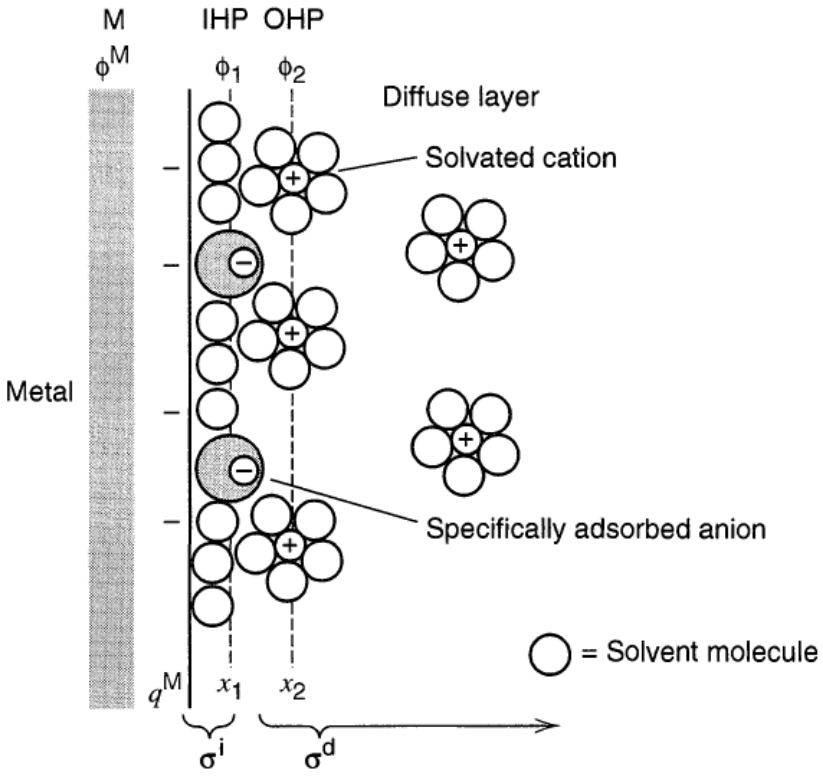

Figure 6. Proposed model of the double layer region under conditions where anions are specifically adsorbed [23,29].

potential decreases linearly from the surface of the electrode to the IHP, and the potential decreases exponentially from the IHP to the OHP [23,29,53,54]. The solvent and the adsorbed layers determine the proximate of the species to the electrode surface. If the solvent is strongly absorbed, electroactive species can only approach the surface up to the OHP. Since the maximum potential resides at the solid-liquid interface, electroactive species at a greater distance than x_0 experience a lesser potential. The lower potential is called a potential drop, and the amount is determined by $\phi_2 - \phi^S$. The ability of the electroactive species to be oxidized or reduced is determined by the potential of the electrode. For example, Cu^{2+} is reduced to Cu^{+} at 0.153 V vs. SHE, or Cu^{2+} is reduced $Cu_{(s)}$ at 0.342 V vs. SHE. Therefore, the electrochemical process is dependent on the potential of the electrode and the distance of the species to the electrode surface.

2.3 Potential-step coulometry

In the potential-step coulometry method, a constant potential is applied to the working electrode until the entire electroactive specie is quantitatively oxidized or reduced [53,54]. In thin-layer electrochemistry, the electroactive species are oxidized or reduced instantly, so the current is initially high for 1 or 2 seconds. This rapid electrochemical reaction is the result of a thin-layer solution on the electrode surface. The electroactive species are not limited by diffusion (migration) as compare to species in bulk solution. Eventually, the current rapidly decreases close to zero. The charge can be measured by the following equation:

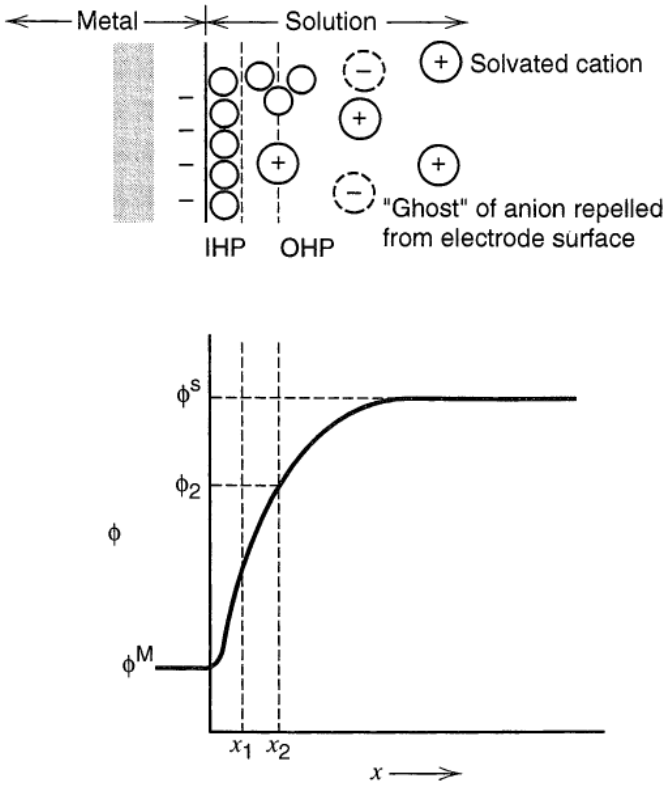

Figure 7. Potential profile across the double-layer in the absence of specific adsorption of ions. The variable ϕ is called the inner potential. A model of the double layer region under conditions where anions are specifically adsorbed [23].

$$Q - Q_b = nFA\Gamma \quad (21)$$

where Q is the charge of the oxidation or reduction in coulombs, Q_b is the charge of the supporting electrolyte in coulombs, n is the number of electron transferred, F is Faraday's constant, A is the area of the electrode, is the surface coverage. Faraday's law relates the Q to the number of moles of the analyte:

$$Q = nFn_a \quad (22)$$

where n is the number of moles of electrons in the analyte half-reaction, F is the Faradaic constant (96485.34 C/mol), and n_a is the number of moles of the analyte.

2.4 Volume of thin-layer Cell

Potential step coulometry is used to measure the volume of the thin-layer cavity. The cavity is filled with a 2.0 mM (know to four significant figures) Fe^{2+} in 1.0 M H_2SO_4. A potential between 0.2 V and 0.50V is applied for the Fe^{2+}/Fe^{3+} redox couple:

$$Fe^{2+} \rightarrow Fe^{3+} + e- \quad (23)$$

The volume of the thin-layer cavity, due to the charge, can be extracted from by Faraday's law:

$$V = Q/nFC \quad (24)$$

Where V is the volume of the thin-layer cavity, Q is the charge of the oxidation or reduction, n is the number of electrons transferred during the electrochemical reaction, F is the Faradaic constant (96485.34 C/mol), and C is the concentration of the solute.

2.5 Cyclic voltammetry

In cyclic voltammetry, the triangular waveform shown in Figure 8a is applied to the working electrode [23,53,54]. A linear potential ramp between times t_0 and t_1 typically lasts several seconds. At time t_1, the ramp is reversed to bring the potential

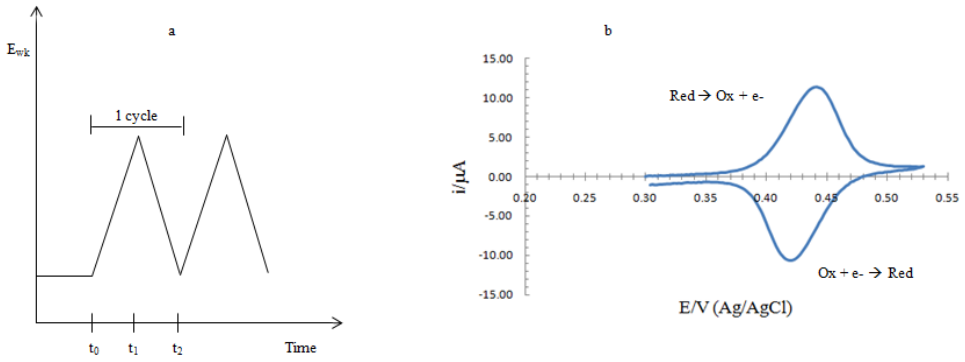

Figure 8. (a) Waveform used in cyclic voltammetry, and (b) a typical cyclic voltammogram.

back to its initial values at the time t_2. The cycle may be repeated several times. During the potential sweep, the electroanalytical instrument measures the current resulting fromthe applied potential. The resulting plot of current I vs. potential E is called a cyclic voltammogram (CV). Figure 8b illustrates, in a schematic way, the cyclic voltammogram measured for a reversible redox process Red $\rightleftharpoons$ Ox + ne- taking place at the surface of a solid electrode for thin-layer cell. As the applied potential approaches the characteristic standard potential E^0 for the redox couple Ox/Red, a current begins to increase until a peak is reached. The current decreases after the peak because analyte becomes depleted in the thin-layer cavity due to the reaction Red $\rightleftharpoons$ Ox + ne-. For a reversible electrode process, the peak current i_p = is proportional to the concentration of the analyte and the scan rate according to the Equation 26:

$$i_p = n^2 F^2 V(-r) C_o / 4RT \qquad (25)$$

Where n is the number of electrons exchanged in the electrode process, F is Faraday's constant, V is the volume of the thin-layer, and r is the potential scan rate (V/s), and C_o is the concentration of the oxidized specie [23,54]. By integrating the area under the current potential curve (charge = current x time), cyclic voltammetry can also be used to measure the amount of electroactivity.

In this research, a H-cell cell and thin-layer cell were used as showed in Figure 5a. The H-cell contained a working electrode compartment and reference compartment. Thin-layer cell with the Pd billet (working electrode) in the cavity was placed in the

working electrode compartment. The reference and the auxiliary electrode were placed in the reference compartment. The reference electrode is a Ag/AgCl (1.0 M NaCl), and the auxiliary electrode is a Pt wire. The potentiostat is a BAS CV-27 (Bioanalytical System Inc., West Lafayette, IN). The supporting electrolyte was 1.0 M H_2SO_4 (Aldrich Chemicals, Milwauke, WI).

2.6 Clean polycrystalline Pd electrode

Figure 9 shows the CV measured for the reversible electrode process $Ox + ne- \rightleftharpoons Red$ at the surface of polycrystalline Pd surface in 1.0 M H_2SO_4. At the initial potential of 0.2 V, the small anodic current produces trace impurities (e.g. oxygen). As the applied potential approaches 0.45 V, a current begins to increase until a semi-plateau is formed. The CV shows two peaks at 0.6 V and 0.8 V. The surface oxidation of Pd is described by the electrochemical reactions [24]:

$$Pd + H_2O \rightarrow Pd\text{-}OH_{(s)} + H^+ + e^- \quad (26)$$

$$Pd\text{-}OH_{(s)} \rightarrow Pd\text{-}O_{(s)} + H^+ + e- \quad (27)$$

The extent of the surface oxidation might be similar to Pt with a two monolayer oxide film [55].

The increase in the anodic current at 1.0V is the oxygen evolution from the oxidation of water:

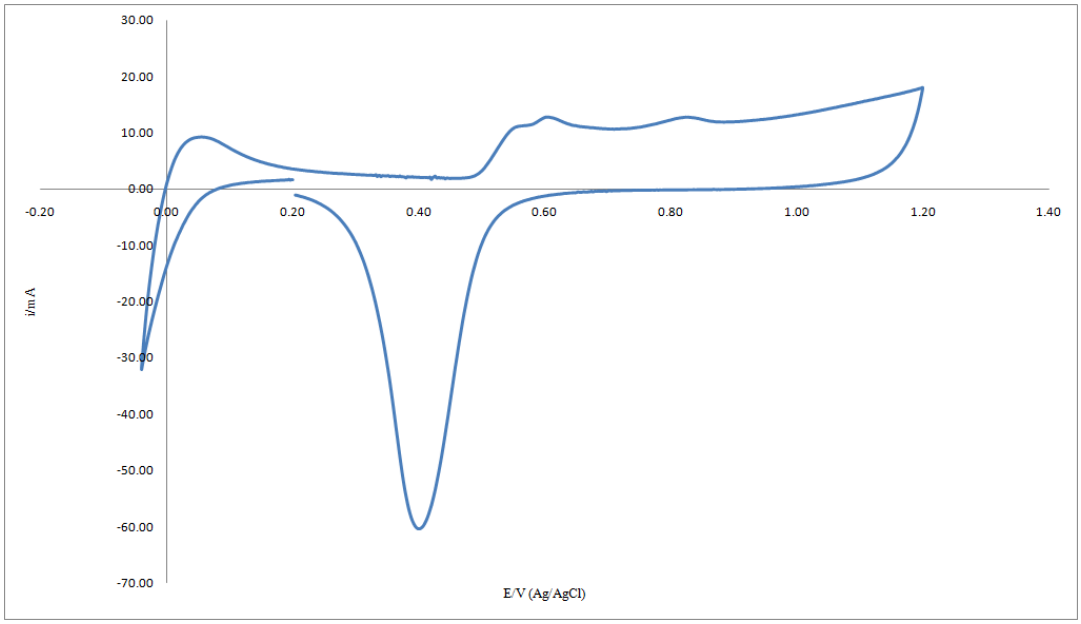

Figure 9. Cyclic voltammogram of clean polycrystalline Pd recorded in 1.0 M H2SO4 solution. Scan rate, 2 mV/s.

$$2H_2O_{(l)} \rightarrow O_{2(g)} + 4H^+_{(aq)} + 4e^-_{(aq)} \quad (28)$$

When the potential sweep is reversed at 1.2 V, the current is decreased to zero. The onset of surface reduction occurs at 0.6 V until the cathodic current decreases to a double layer current. At 0 V, the CV shows the onset of hydrogen evolution:

$$2H_2O_{(l)} \rightarrow H_{2(g)} + 2OH^-_{(aq)} \quad (29)$$

2.7 Surface coverage

Since the chemisorbed molecule, such as hydroquinone, is redox inactive, the measurements of surface coverage (Γ = nmol/cm^2) was obtained from the difference in charge from the unadsorbed molecules. The Γ was used to determine the experimental cross-section, σ_{ex}, of the adsorbed molecule. The molecular cross-section is given by the following equation:

$$\sigma_{ex} = \text{Å}^2/\text{molecule} = 10^{16}/(N_A\Gamma) \quad (30)$$

where N_A is Avogadro's number [40,56]. The σ_{ex} was compared to various calculated cross-section (σ_{cal}) of the molecule to determine the surface orientation.

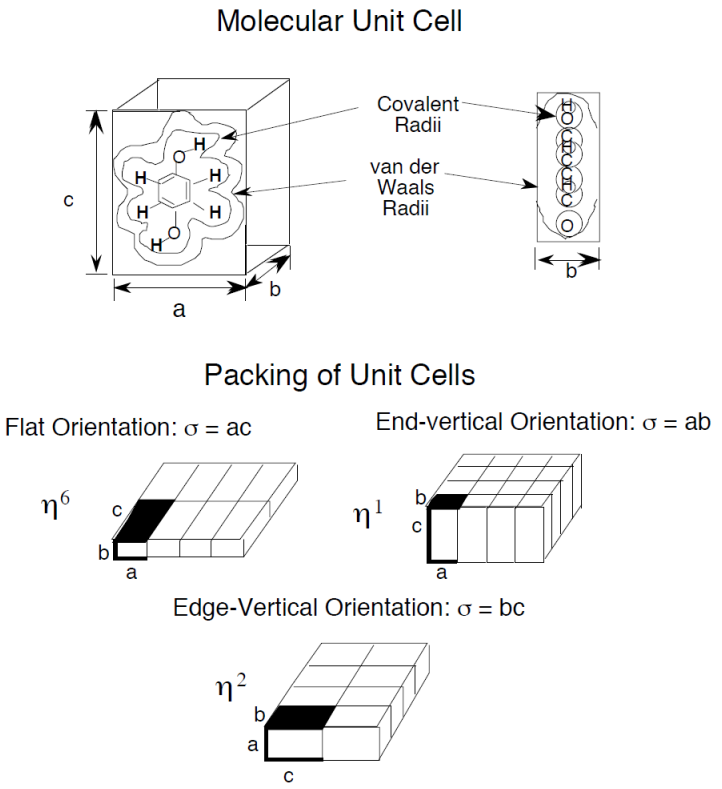

Figure 10. Molecular unit cell adopted in the calculation of the adsorbed molecule cross-section [56].

In order to determined the σ_{cal} occupied by an adsorbed molecule, the molecule was enclosed in a rectangular parallelepiped unit cell with one of the cross-section area parallel to the electrode surface as illustrated in Figure 10. The sized of the unit cell was determined from the structure of the molecule. The molecule was constructed from the covalent and Van der Waals radii of the atoms tabulated by Pauling and the appropriate bond angles between atoms [57]. The length, width, and thickness of the unit cell were obtained from molecule. The length was established from the longest axis passing through the center of the ring. The width was the sum of the length from atomic radii protruding along the axis perpendicular to the length of the molecule. The thickness was established from thickest point from the longest axis.

Hubbard and co-workers, with the use of thin-layer electrochemistry (TLE), determined the orientation of aromatic compounds on Pt, Au, and Ir electrodes [45,46,58,59]. The adsorbate orientation is indirectly measured from the surface coverage (Γ = nmol/cm^2), and the conversion of Γ to molecular cross-sections (σ_{ex} = Å^2/molecule= $10^{16}/(N_A\Gamma)$ for comparison with all possible molar orientations [46]. In the TLE technique, the cavity is filled once with one aliquot of a precise molar amount of adsorbate. A portion of the molecules is adsorbed on the clean Pd electrode as shown in Figure 11 (blue). This surface reaction results in a cavity with a molar concentration (C) of less than the bulk concentration (C^o):

$$VC = VC^o - A\Gamma \tag{31}$$

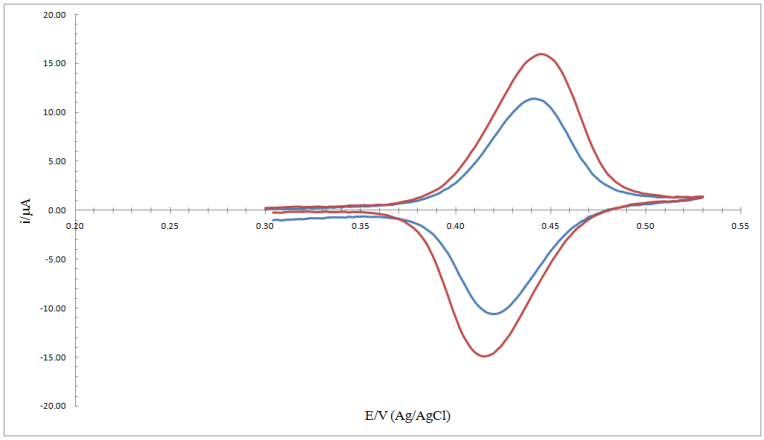

Figure 11. Cyclic voltammogram of 0.5 mM of hydroquinone after one aliquot (blue) and a second aliquot (red) recorded in 1.0 M H_2SO_4 solution. Scan rate, 2 mV/s.

where V is the volume of the cavity (5.48 μL), A is the surface area of the Pd electrode (1.27 cm^2), and Γ is the surface coverage ($nmol/cm^2$) of the adsorbed solute molecule. If the potential region for electrochemical reactivity is different for the adsorbed species, than unadsorbed species is determined by modifying Faraday's law (23) to include the surface adsorption:

$$Q_1 - Q_{1b} = nFVC = nFVC^o - nFA\Gamma \quad (32)$$

Where Q_1 denotes the electrolytic charge observed for a single filling of the thin layer cavity, Q_{1b} is the background electrolytic charge consumed in an otherwise identical experiment in which the dissolved reactant has been rinsed from the cell, and *n* is the number of electrons consumed per molecule of reactant [56,60-62]. Since all the chemisorption occurs at the first aliquot, the second aliquot (or multiple aliquots) results in the concentration in the thin-layer cavity to equal the concentration of bulk solution as shown in Figure 10 (red). The electrolytic charge of the unadsorbed solute in the cavity after the second aliquot is given by:

$$Q - Q_b = nFVC^o \quad (33)$$

If Q_b and Q_{1b} are not equal, Equations 5 and 6 can be combined to give the surface coverage (Γ):

$$\Gamma = (Q - Q_{1b}) - (Q_1 - Q_b)/nFA \quad (34)$$

If Q_b and Q_{1b} are equal, equation 34 can be simplified to:

$$\Gamma = (Q - Q_1)/nFA \quad (35)$$

In very dilute solutions (< 0.1 mM), several aliquots of solution are required to completely saturate the surface with adsorbate. Therefore, all of the solute in the first aliquot is adsorbed on the surface, and the surface coverage is given by the equation:

$$\Gamma_1 = VC^o/A \quad (36)$$

To achieve full coverage, the addition of multiple (k) aliquots is required. The surface coverage up to the n^{th} aliquot is given by:

$$\Gamma_1 + \Gamma_2 + \Gamma_3 \ldots = kVC^o/A \quad (37)$$

If complete adsorption is attained only after k aliquots, an additional (k + 1) aliquot will be necessary to measure the final increment of surface coverage:

$$\Gamma_{k+1} = (Q_{k+1} - Q_k)/nFA \quad (38)$$

The total coverage will be [63]:

$$\Gamma = \sum_{i=1}^{k+1} i \tag{39}$$

Q_{k+1} is equal to the bulk solute concentration by the following equation:

$$C^o = (Q_{k+1} - Q_b)/nFV \tag{40}$$

3. RESULTS AND DISCUSSION

3.1 Hydroquinone and benzoquinone

Hydroquinone and benzoquinone were used to obtain a better understanding of the adsorption of quinones at the surface of the polycrystalline Pd electrodes. Hydroquinone is an ideal species for qualitative and quantitative investigations of adsorbate-substrate interactions because the potential for the redox reaction of unadsorbed hydroquinone is different from that of the adsorbed species. Figure 12 shows cyclic voltammograms (CVs) of a clean polycrystalline Pd electrode in 1.0 M H_2SO_4 with and without 1.0 mM hydroquinone. In the absence of hydroquinone, the CV in Figure 12 shows a typical example for a clean polycrystalline Pd electrode with several distinct anodic peaks at positive potentials. The shape of the CV is identical to those reported in published literature [46,60,64]. Both curves in Figure 12, which were obtained after the introduction of the first and second aliquot of 1.0 mM hydroquinone in 1.0 M H_2SO_4 solution into the thin-layer cavity, show a peak at ca. 0.45 V. Both curves in Figure 12, which were obtained after the introduction of the first and second aliquot of 1.0 mM hydroquinone in 1.0 M H_2SO_4 solution into the cavity, show a peak at ca. 0.45 V.

This indicates that the large oxidation peak at ca. 0.8 V is due only to the chemisorbed organic. Earlier it was described that anodic oxidation at this potential occurs only when the adsorbate is chemisorbed on the surface; no such oxidation occurs for the unadsorbed specie. It should be noted that the large anodic peak includes the

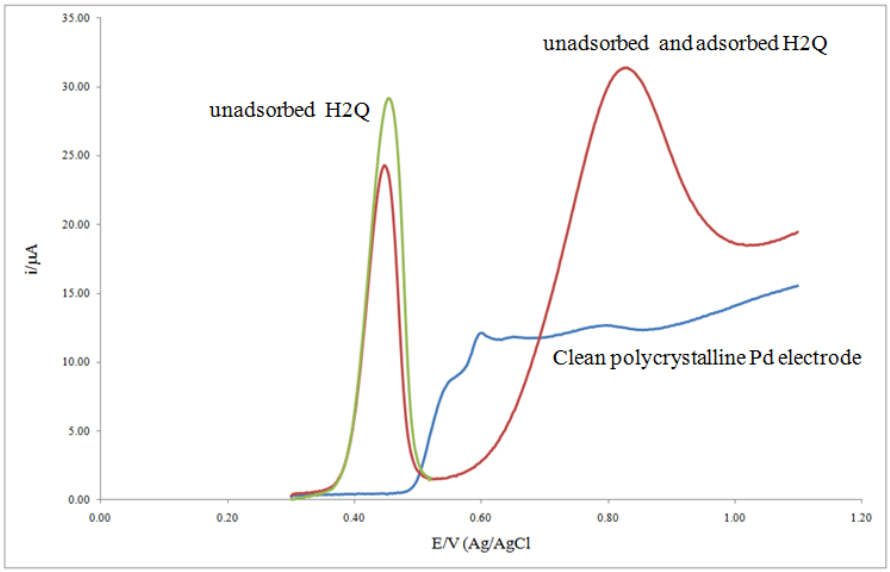

Figure 12. Linear sweep voltammograms for the anodic oxidation of H_2Q chemisorbed at a Pd thin-layer electrode with and without the solute H_2Q (1.0 mM) in 1.0 M H_2SO_4. Scan rate, 2.0 mV/s.

oxidation of the metal surface to the oxide; this happens only after the surface organic is oxidatively destroyed.

Figure 13 shows chemisorption isotherms (Γ-vs-pC plots where pC = -log C) of hydroquinone and benzoquinone. The isotherms of both species are essentially identical. The isotherms at Pd are also similar to those at polycrystalline Pt electrode, except that, at low concentrations, the plateau for Pd is not as sharp as that at Pt, and the transition from the lower Γ–plateau to the upper Γ–plateau is less abrupt than that for Pt.
The two isotherm plateaus of the species at the Pd electrode give identical information for the molecular orientation in the chemisorbed layer as the plateaus of those at Pt electrodes. The lower Γ–plateau indicates a parallel (η^6) orientation of hydroquinone and benzoquinone at the Pd electrode at low concentrations, while the upper Γ–plateau suggests an edge-wise (η^2) orientation of the adsorbing compounds at high concentrations ($C^0 > 0.8$ mM). Both orientations on Pt surfaces have been found to be consistent with several studies based on surface coverage measurements, including infrared reflection-absorption spectroscopy (IRRAS), high- resolution electron energy loss spectroscopy (HREELS), and scanning tunneling microscopy (STM) [33,65,66].

The adsorbate molecular orientations for both hydroquinone and benzoquinone at the lower and upper Γ–plateaus were determined by comparing the experimental cross-sections, $\sigma_{exp} = A^2/\text{molecule} = 10^{16}/(N_A\Gamma)$, with calculated cross-sections. At low concentrations, for hydroquinone, the surface coverage, Γ, of 0.37 nmol/cm^2 corresponds to an experimental cross-section, σ_{exp}, of 44.9 Å^2; for benzoquinone, the σ_{exp} is 43.7 Å^2. Both cross-sections correspond to some of the following calculated cross-sections shown

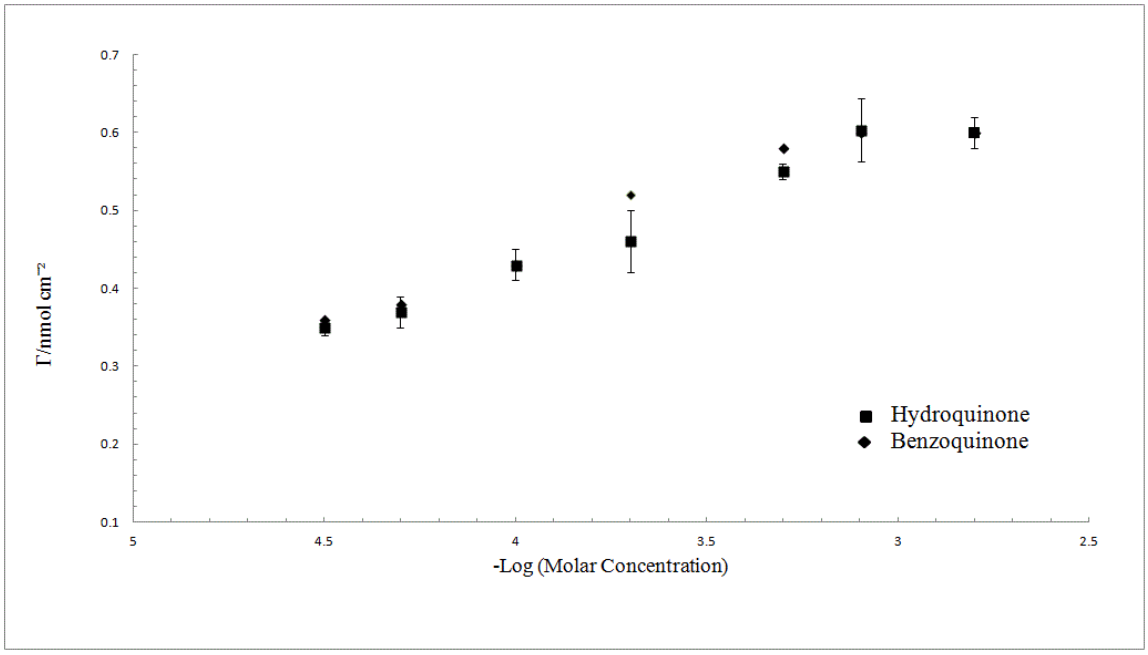

Figure 13. Chemisorption isotherms of hydroquinone and benzoquinone at a smooth polycrystalline palladium electrode after subjecting the electrode to different solute concentrations. Supporting electrolyte, 1 M H_2SO_4. Volume of thin-layer cell, 5.48 μL, electrode surface area, 1.27 cm^2, temperature, T = 298 K.

in Figure 14.

The two σ_{exp} values are smaller than the calculated cross-sections of 53.8 $Å^2$ (hydroquinone) and 52.5 $Å^2$ (benzoquinone) for the η^6-orientation. The lower-than-expected σ_{exp} seems to indicate the presence of an adsorbate with an orientation that is not completely parallel to the surface.

Figure 15 shows the HREELS spectra of a Pd(100) surface after immersion in 1 mM hydroquinone and 1 mM benzoquinone in H_2SO_4 [47]. The analysis of these spectra shows the presence of the out-of-plane C-H bend, in-plane bends, and in-plane stretches. The importance of the in-plane bends and stretches is limited by the metal surface selection rule in which only oscillating dipole perpendicular to the metal surface is IR active [1,19]. When the charged specie is located on top of the metal surface, it produces an image dipole of equal size and opposite sign within the surface as a consequence of the free-moving electrons from the conduction-band as shown in Figure 16 a [1,19]. If a dipole is parallel to the surface, the net change in the dipole moment gets canceled by the image dipole preventing the adsorption of IR radiation or electron beam (Figure 16b). In contrast, the dipole moment perpendicular to the metal surface is unaffected by the image dipole, so the vibration is free to interact with the incident energy or electron beam (Figure 16c) [1,19]. If the molecule was completely parallel to the Pd surface, the

out-of-pane bend would have been the only loss peak. The parallel orientation can also be confirmed from the absence the distinct C-H at around 3000 cm^{-1} [40]. The appearance of the in-plane vibrational modes indicates an adsorbed molecule with a slightly tilted orientation. Another feature of the spectra is the identical loss peaks for

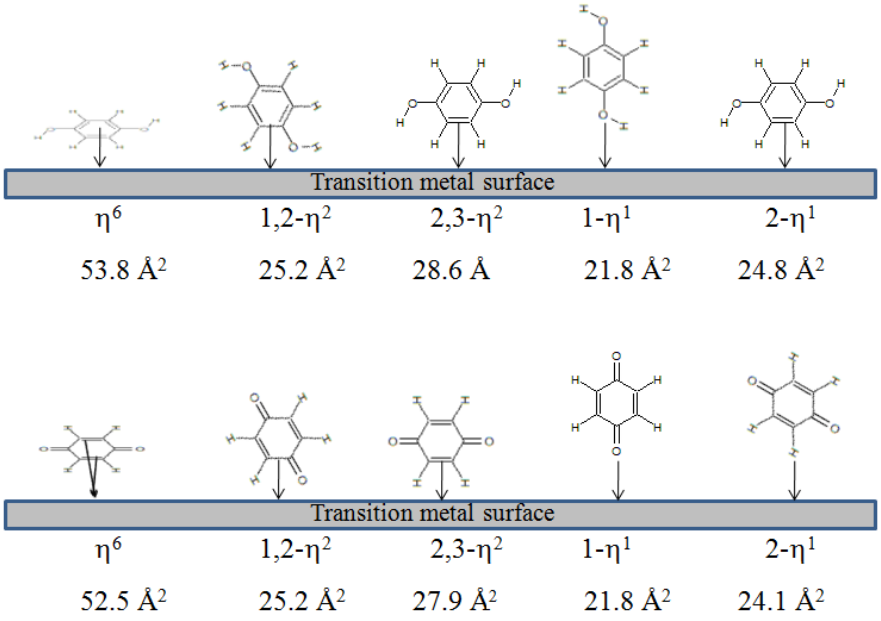

Figure 14. Mode of adsorption and calculated cross-sections for hydroquinone and benzoquinone on a metal surface.

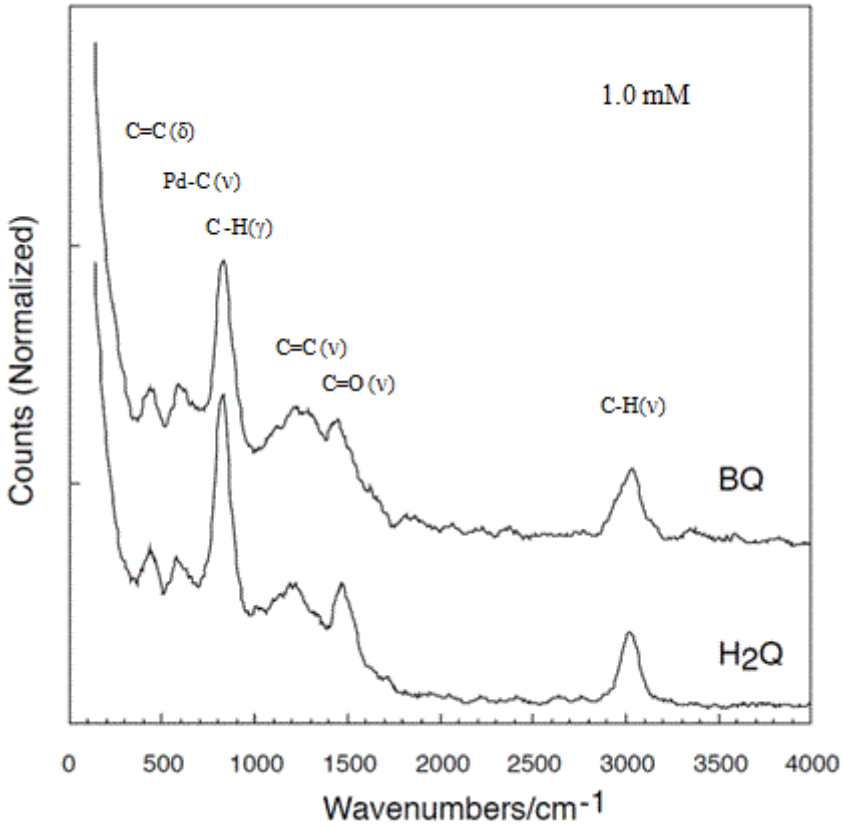

Figure 15. HREELS spectra of Pd(100) surfaces after emersion from a 1 mM BQ in 10 mM H_2SO_4 and 1mM H_2Q in 10 mM H_2SO_4 solution [41].

hydroquinone and benzoquinone. Also, The spectrum of hydroquinone lacks a peak at 3500 cm^{-1} for O-H stretching and the peak at 1474 cm^{-1}corresponds to a C=O stretch. These results were also identical at concentrations less than 1 mM (0.02, 0.1, 0.04 mM) [48,52]. Therefore, hydroquinone at low concentration is adsorbed as benzoquinone while the benzoquinone remains intact after chemisorption [47]. These vibrational modes are similar to those observed in the IR spectra for unadsorbed and adsorbed benzoquinone [66]. Furthermore, Scanning tunneling microscopy (STM) also confirms the slightly tilted flat orientation for benzene and hydroquinone onto Pd electrodes [67,68].

Itaya and coworkers also studied the adsorption of organic compounds on single crystal metal electrodes [33,37,38,69]. Images retrieved by scanning tunneling microscopy (STM) revealed the presence of adsorbed molecules with flat orientations. The flat orientation (η^6) of benzene, pyridine, and 1,4-dimethylbenzene at low concentrations has also been observed on single crystal electrodes such as Au(111), Rh(111), Pt(111), and Cu(111) [34,38,70,71].

In the low concentration regime ($C < 10^{-4}$ M), hydroquinone is oxidatively chemisorbed with a flat orientation on the surface to form benzoquinone and H_2 gas. This irreversible chemisorption is similar for benzoquinone at low concentrations except that benzoquinone is not oxidized. The reaction between hydroquinone (or benzoquinone) and the Pd surface can be represented by the following reactions:

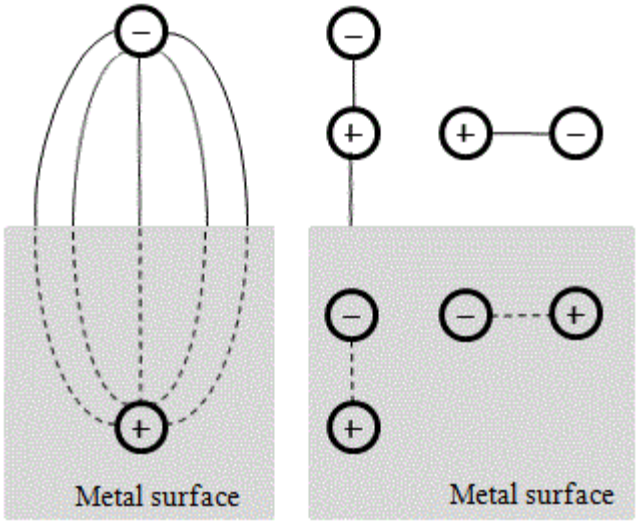

Figure 16. Image dipole at a metallic surface [1].

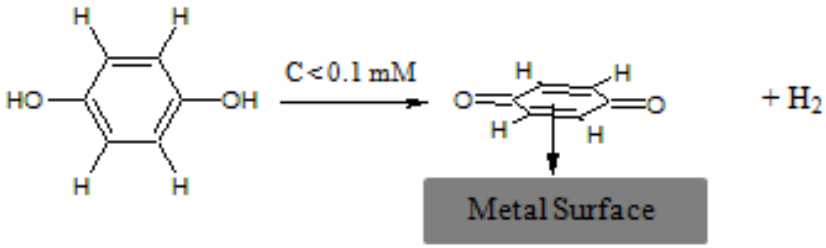

(41)

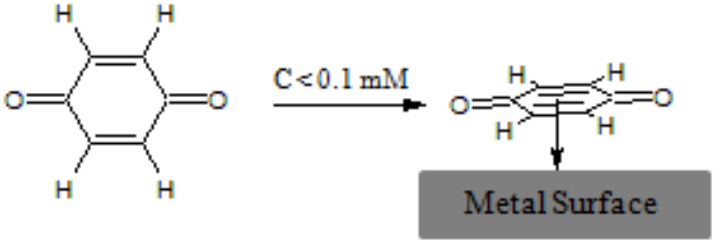

(42)

The interaction between the adsorbate and the Pd surface takes place through the π-system of the quinonoid ring.

In the upper high-concentration plateau, the surface coverage measurements determined a σ_{exp} = 27.2 Å^2 for hydroquinone and σ_{exp} = 27.6 Å^2 for benzoquinone. For hydroquinone, the cross-section is similar to the calculated σ = 28.6 Å^2 for the edge-wise 2,3-η^2 orientation. In the adsorption of benzoquinone, the σ_{exp} is almost identical to the 27.9 Å^2 for a 2,3-η^2 structure**.** HREELS spectra confirms the presence of C=O stretching at 1500 cm^{-1} for hydroquinone adsorbed onto Pd(100) surfaces at various concentrations (1.0, 10.0 and 100.0 mM) [48]. The surface reaction, however, is different when a Pt electrode is used. At concentrations higher than 1 mM, the two C=O groups for hydroquinone are reduced to O-H. Over all, the adsorption of hydroquinone or

benzoquinone results in a 2,3-η^2 structure with only benzoquinone on the surface. The surface reaction for both compounds is as follows:

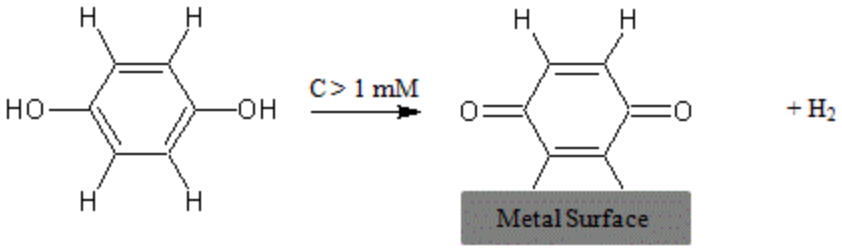

(43)

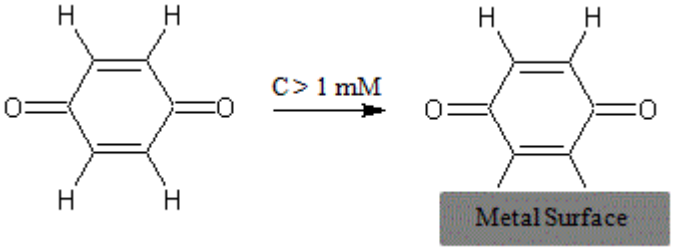

(44)

3.2 Hydroquinone substituted with methyl groups

The chemisorption isotherms of methylhydroquinone (MH_2Q) , 2,3-dimethylhydroquinone (DMH_2Q), and 2,3,5-trimethylhydroquinone (TMH_2Q) are shown in Figure 17. All three isotherms are almost identical except at 0.03 mM. At concentrations below 0.1 mM, MH_2Q and DMH_2Q have the absence of a Γ-plateau. These results are similar to H_2Q and BQ. The Γ-plateau at low concentrations for TMH_2Q is similar to the results for 2,5-dimethylhydroquinone on a polycrystalline Pt electrode [56,60]. The presence of methyl groups at the quinone edges seems to retard

the transition from a flat to an edgewise orientation [40]. This particular behavior on the adsorption process is more profound for durohydroquinone (2,3,5,6-tetramethylhydoquinone); since quinoneedges contain methyl groups, durohydroquinone only has a flat orientation at 0.03 mM and 0.3 mM [40]. At concentrations higher than 0.05 mM, the isotherms are basically identical for the three adsorbates unlike the isotherms for Pt [62].

The adsorption at different concentrations was also studied by HREELS. Figures 18 and 19 show the HREELS spectra of 2,3-dimethylbenzoquinone (DMBQ) and 2,3,5-trimethylbenzoquinone (TMBQ) after exposing the Pd(111) electrode to 0.05 mM, 0.5 mM, and 5.0 mM solutions of 2,3-DMH_2Q and 2,3,5-TMH_2Q. The HREELS spectra show the presence of the loss peaks for the in-plane stretching vibrations ν(C-H) at 3000 cm^{-1} and ν(C=O) at 1480 cm^{-1}. The spectra also show the absence of the loss peak for the in-plane stretching vibration ν(O-H) at 3500 cm^{-1}. The presence of a C=O stretch indicates oxidative chemisorption of the phenolic groups from solute DMH_2Q and TMH_2Q to benzoquinone moieties. These results suggest an unhindered surface activity for the oxidation of the H_2Q moiety by the methyl groups. This result is not surprising because hydroquinone also shows an identical chemisorption process at low concentrations on Pt and Pd [46,72]. The oxidative chemisorption on Pd, however, is different from that on the Pt electrode. For Pt, the loss of the two electrons and two protons is limited to concentrations below 1 mM [60]. The C-H and the C=O stretching also give additional information about the adsorbate-substrate interaction. Since the surface metal selection rule requires a vibrational mode perpendicular to the surface to

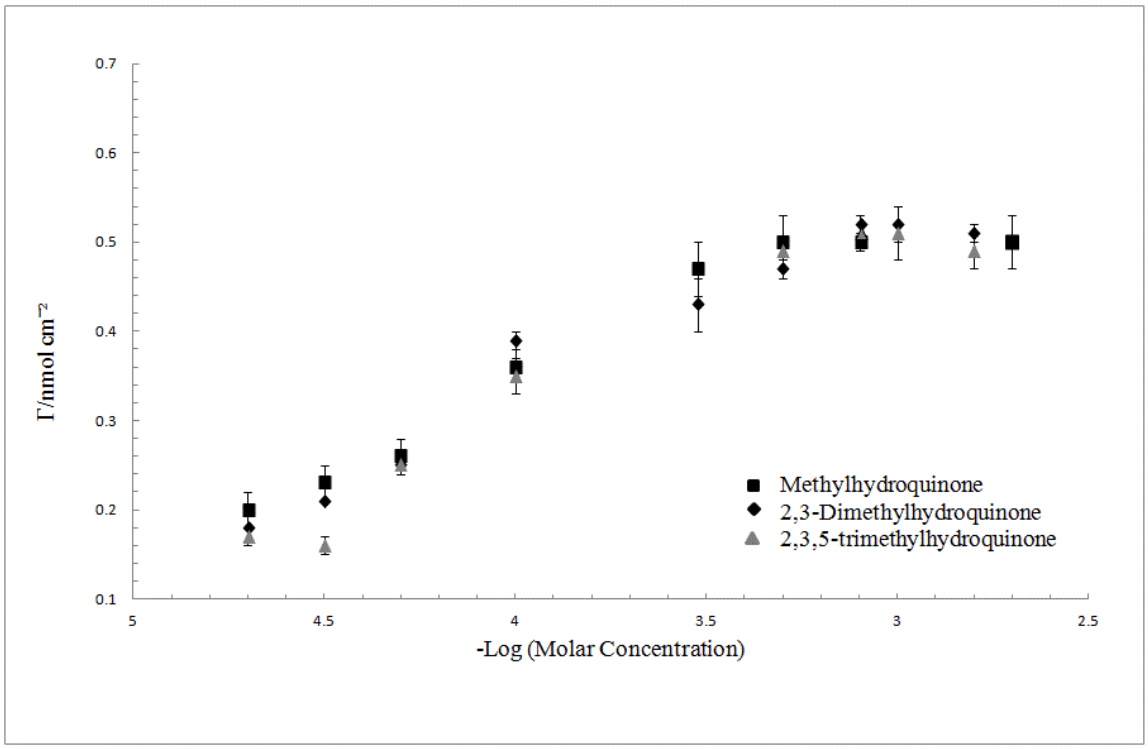

Figure 17. Chemisorption isotherms of hydroquinone derivatives at a smooth polycrystalline palladium electrode after subjecting the electrode to different solute concentrations. Supporting electrolyte, 1 M H_2SO_4, volume of thin-layer cell, 5.48 μL, electrode surface area, 1.27 cm^2, temperature, T = 298 K.

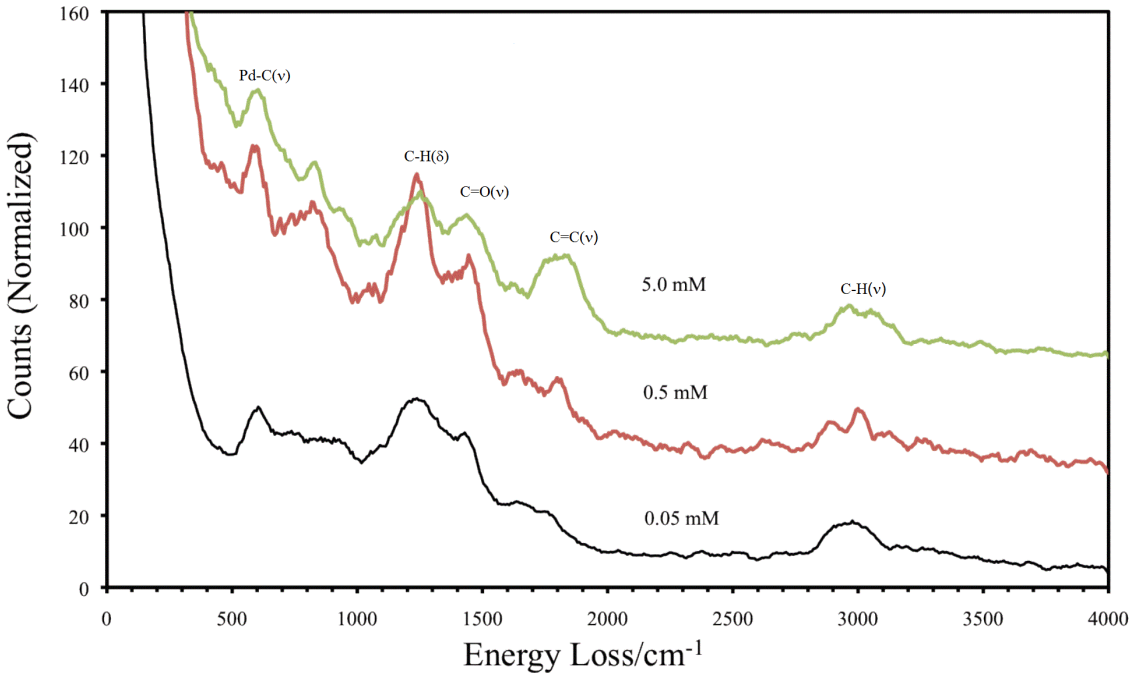

Figure 18. HREELS spectra of the chemisorbed 2,3-dimethylbenzoquinone on Pd(111) surfaces after subjecting the electrode to 0.05 mM, 0.5 mM and 5.0 mM solutions of 2,3-dimethylhydroquione [46].

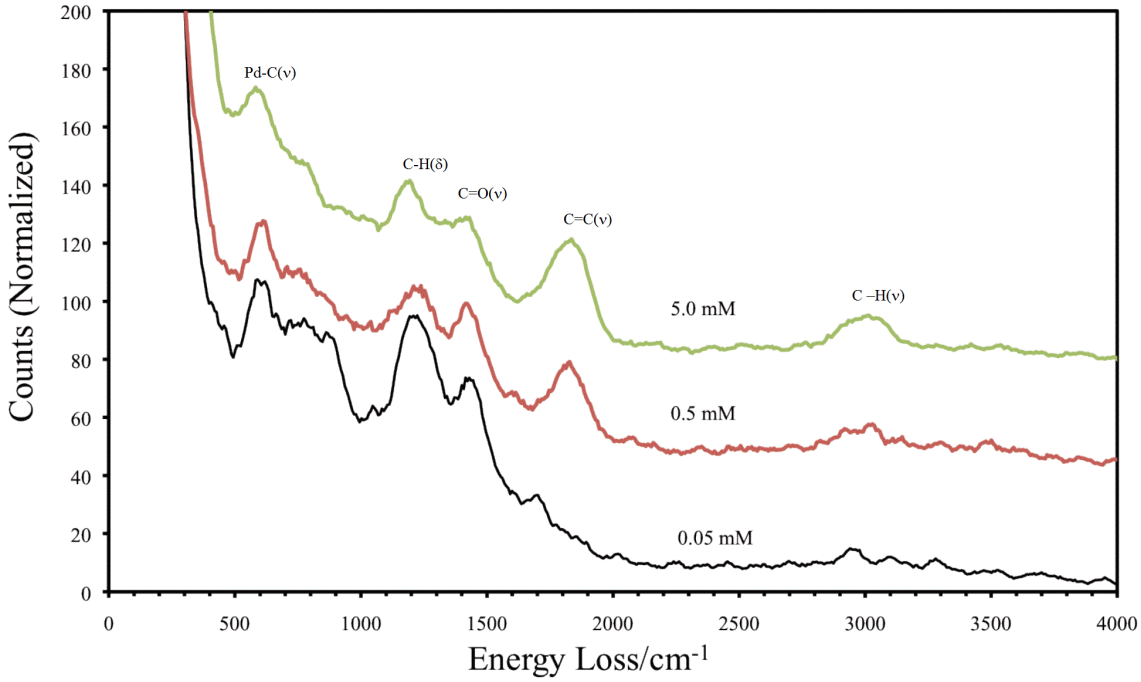

Figure 19. HREELS spectra of chemisorbed 2,3,5-trimethylbenzoquinone on Pd(111) surfaces after subjecting the electrode to 0.05 mM, 0.5 mM and 5.0 mM solutions of 2,3,5-trimethylhydroquinone [46].

be IR active, the two loss peak can only occur if the molecule is not completely flat. A slightly tilt orientation (η^6) orientation with respect to the metal surface is the more likely structure. This structure is not surprising, because the hydroquinone moiety contains large bulky methyl groups.The higher-intensity loss peak at 0.5 mM and 5.0 mM indicates a lack of image–charge effect. The edge-wise (η^2) orientation is the more likely structure as it allows the in-plane vibration and stretching to occur away from the metal surface [14,60].

Since methyl groups are known to donate electron density to the aromatic ring, it was expected that the aromatic ring would prefer the flat orientation by forming a stronger metal-olefin bond [26,27,73]. This stronger interaction in turn should have resulted in a sharper plateau at low concentrations compared to hydroquinone. The effects of the methyl groups can be seen in cyclic voltammetry. This inductive effect tends to lower the oxidation-reduction potential of the unadsorbed diphenol-quinone couples as shown in Figure 20. Each addition of a methyl group reduces the reduction potential wherein 0.41 V, 0.36 V, and 0.29 V were observed for MH_2Q, DMH_2Q, and TMH_2Q,respectively, as compared to 0.46 V for hydroquinone and benzoquinone. In contrast, the oxidation potential of chemisorbed MH_2Q, DMH_2Q, and TMH_2Q is basically identical to 0.88 V. The chemisorption isotherms of MBQ, DMBQ, and TMBQ from MH_2Q, DMH_2Q, and TMH_2Q solutions are very similar as shown in Figure 17. However, theisotherms at low concentrations show an undefined plateau for MBQ and DMBQ, and a plateau for TMBQ. The experimental cross-section was determined

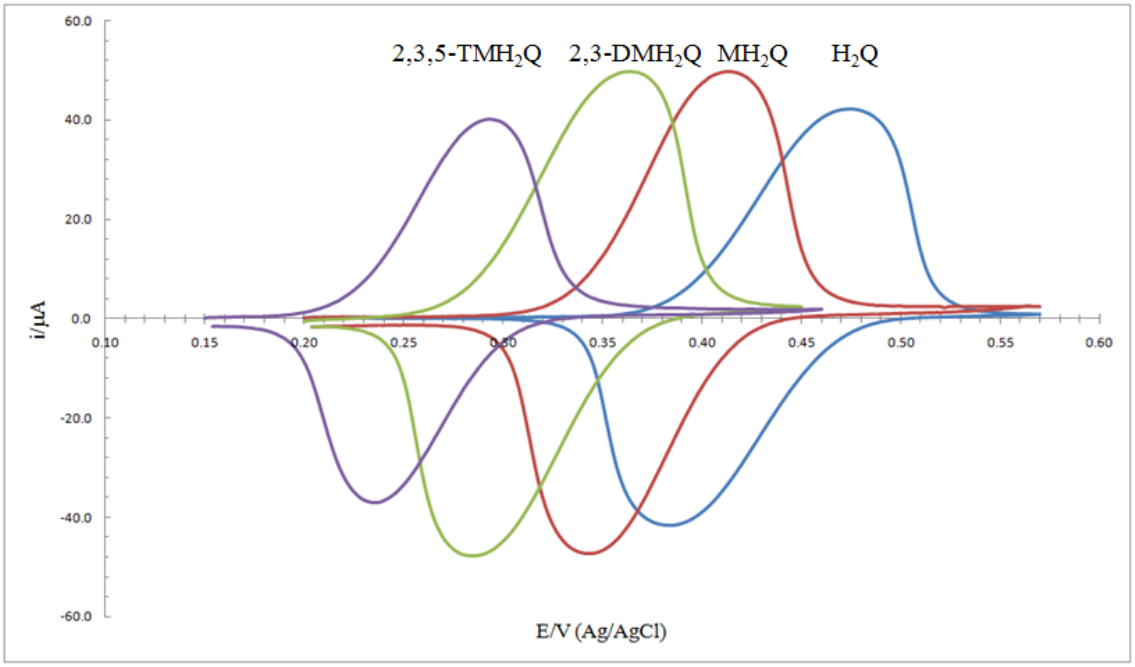

Figure 20. Cyclic voltammograms of hydroquinone and hydroquinone derivatives at similar concentrations in 1.0 M H_2SO_4. Scan rate, 2.0 mV/s.

by the lowest surface coverage value. The Γ of MBQ (Γ = 0.20 nmol/cm^2), DMBQ (Γ = 0.18 nmol/cm^2), and TMBQ (Γ = 0.17 nmol/cm^2) resulted in experimental cross-sections, σ_{ex}, of 83.02 Å^2, 92.24 Å^2, and 97.66 Å^2, respectively. These values do not correspond to any of the calculated σ for the different orientations as shown in Figures 21, 22, and 23. The higher-than-expected σ_{ex} values indicate a weak affinity for the Pd surface. However, these interactions are weak. The lack of chemisorption of alkanes also occurs on the Pt surface [74]. Nevertheless, the HREELS spectra indicate the existence of a η^6-structure with a slight tilt.

The transitions between the lower and upper Γ-plateaus of MBQ, DMBQ, and TMBQ are basically identical to each other as shown in Figure 17. In comparison with the isotherm of hydroquinone, the transitions are less profound for quinones with methyl groups. The methyl groups also tend to facilitate the transition between the flat to edge-wise orientation at lower concentration (0.5 mM) on Pd as compared to Pt electrodes (0.8 mM) [62,75]. The experimental cross section, σ_{ex}, was also calculated from the surface coverage, Γ, at the highest concentration. The σ_{ex} of 33.0 ±2.1 Å^2 for methylhydroquinone points to 1,6-η^2, 3,4-η^2, 2,3-η^2, and 5,6-η^2 structures as shown in Figure 21. In the chemisorption of H_2Q and BQ, as shown in Figure 15, the experimental results indicate the absence of a bond formation from the –OH and C-H groups to the metal surface. Since edge-wise chemisorption on Pd, like Pt, are known for a double C-H activation to form two Pd-C bonds instead of the single dehydrogenation process, a 5,6-η^2 structure is more likely to occur [60]. MBQ has a σ_{ex} of 32.5 ±0.6 Å^2 just like

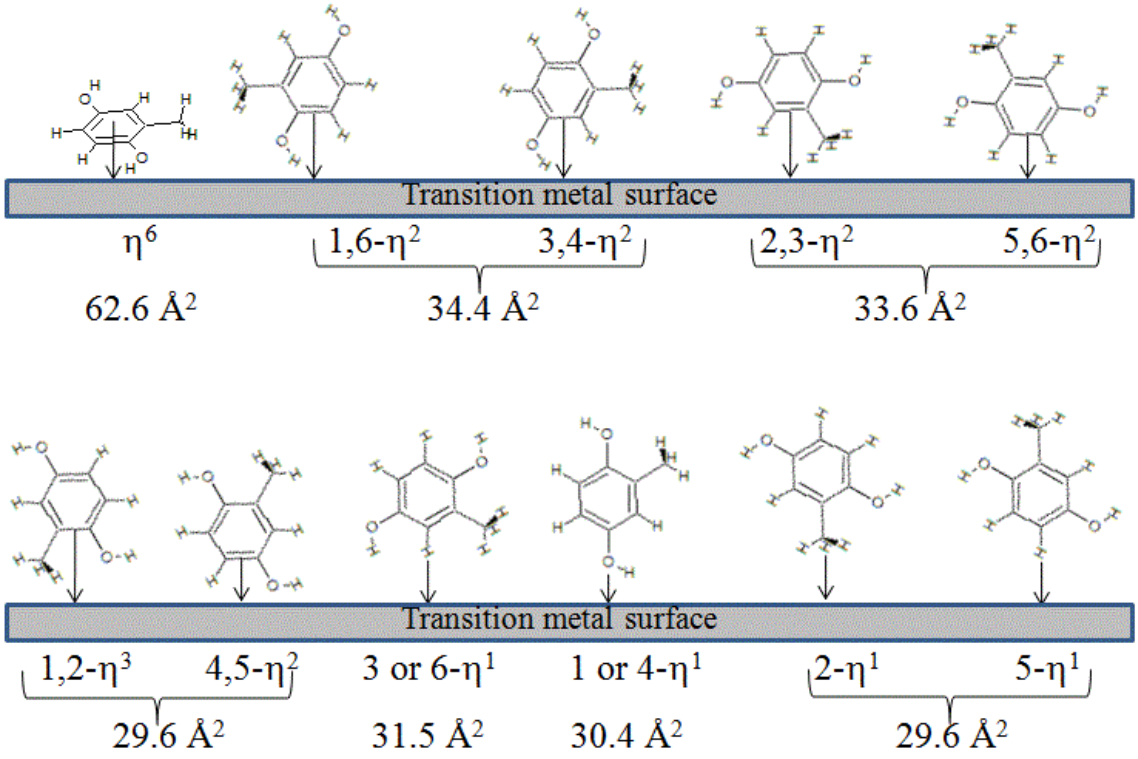

Figure 21. Mode of adsorption and calculated cross-sections of methylhydroquinone on a metal surface.

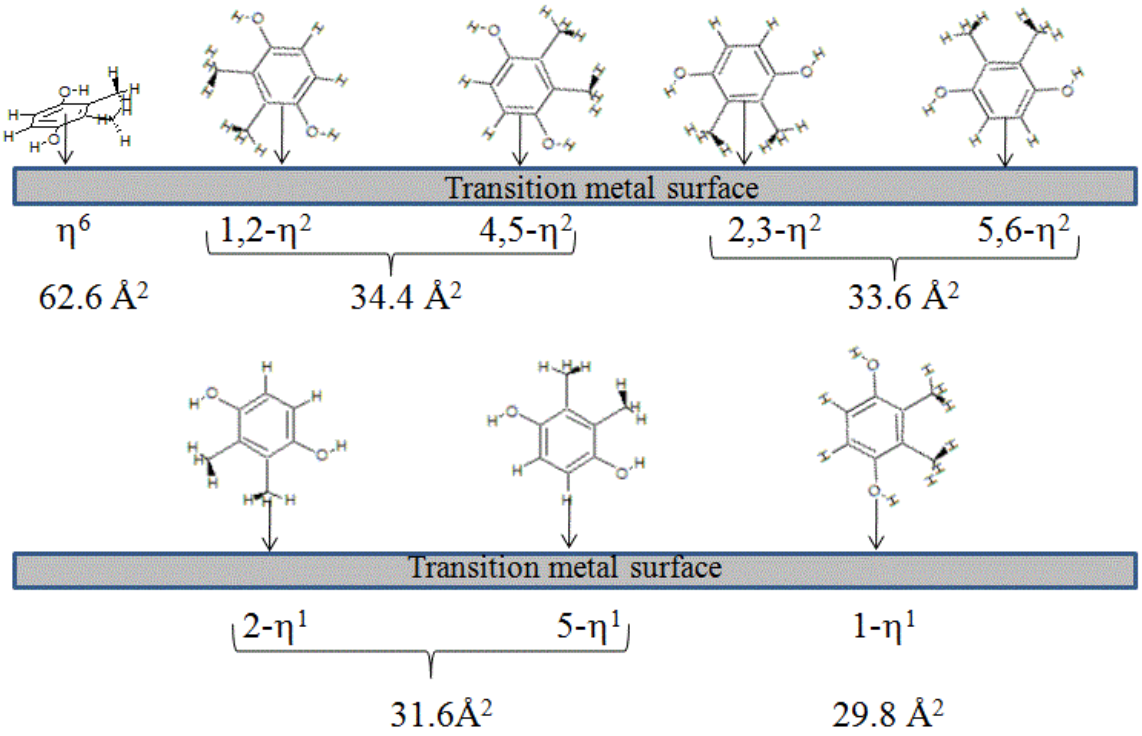

Figure 22. Mode of adsorption and calculated cross-sections of 2,3-dimethylhydroquinone on a metal surface.

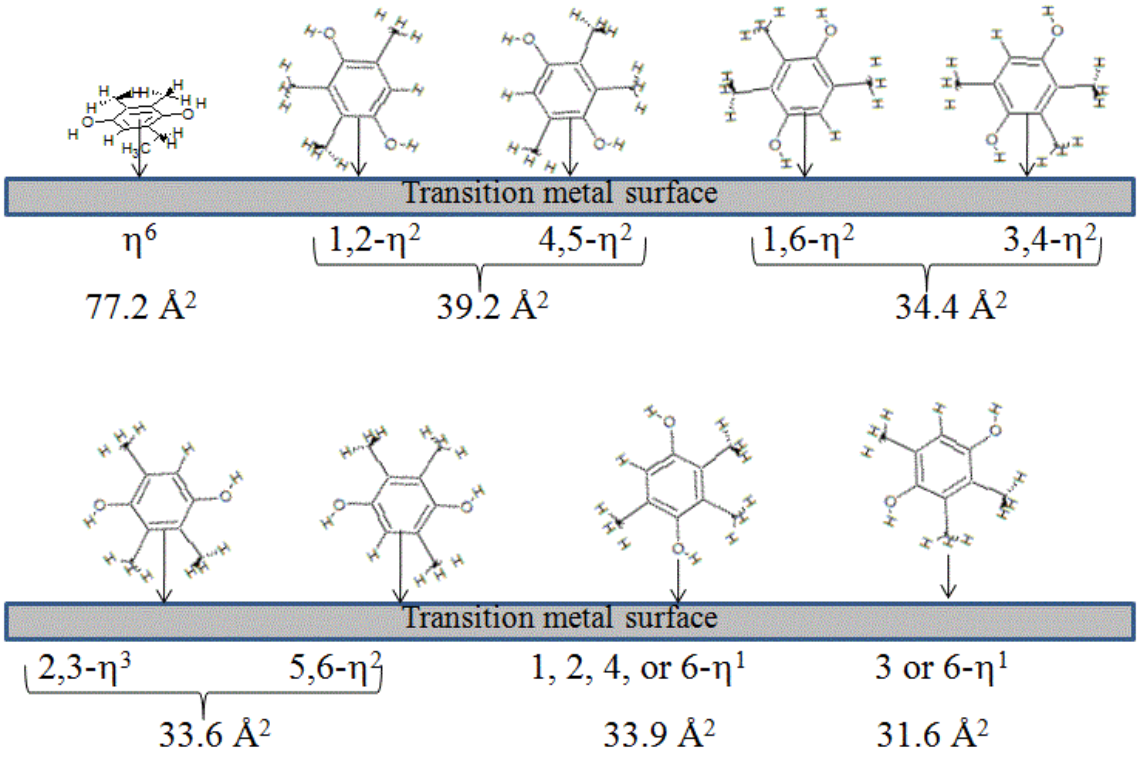

Figure 23. Mode of adsorption and calculated cross-sections of trimethylhydroquinone on a metal surface.

DMBQ has a σ_{ex} of 32.5 ±0.6 Å^2. These values are also closer to the 2,3-η^2 and 5,6-η^2 structures as shown in Figures 21 and 22. The preferred double C-H activation points to a more possible 5,6-η^2 structure. The TMH_2Q has a cross-section of 33.7 ±1.3 Å^2 and this corresponds to 2,3-η^2 and 5,6-η^2 structures as shown in Figure 23. Since a bond formation with a 5,6-η^2 structure might result in an edge-wise orientation with a slight tilt, the 2,3-η^2 is more likely to form on the Pd surface.

3.3 Hydroquinone substituted with sulfonate group

Figure 24 shows the chemisorption isotherm of hydroquinone sulfonic acid (H_2QS) on a polycrystalline Pd electrode. At 0.1 mM, the surface coverage of 0.21 nmol/cm^2 corresponds to a cross section of 70.1 ±0.9 Å^2, which is in the range of acceptable σ_{calc} values for the orientation with a σ_{calc} of 63.4 Å^2. A completely flat orientation is impossible because the sulfonate group is bulkier (2.98 nm) than the thickness of the aromatic ring (2.0 nm) [26,27,57]. H_2QS is more likely to have a slightly tilted flat orientation on the Pd surface. The tilted η^6-structure has been confirmed by HREELS and EC-STM. As in the previous adsorption of hydroquinone derivatives, the adsorption of hydroquinone moiety of at low concentration should occur via the oxidative chemisorption of the phenolic groups. Figure 25 shows the HREELS spectra of benzoquinone sulfonic after the exposure of the Pd(111) surface to 0.05 mM, 0.5 mM, and 5.0 mM solutions of H_2QS. The most important loss peaks are those corresponding

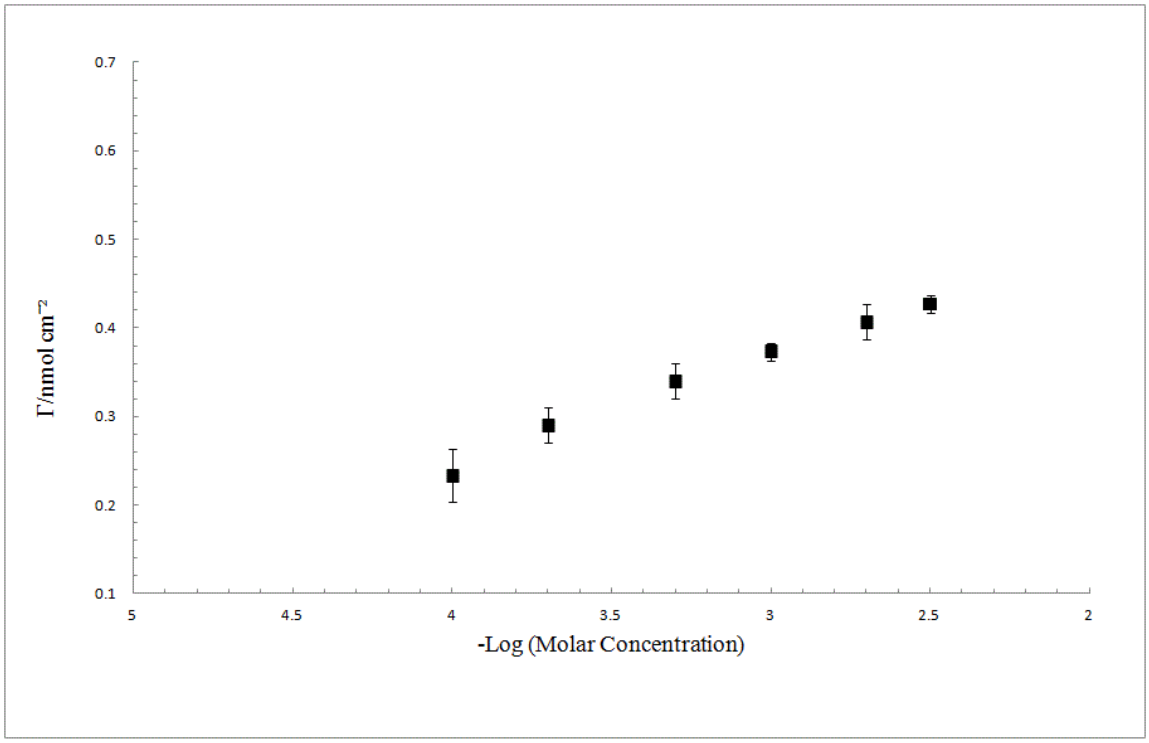

Figure 24. Chemisorption isotherm of hydroquinone sulfonic acid at a smooth polycrystalline palladium electrode after subjecting the electrode to different solute concentrations. Supporting electrolyte, 1 M H_2SO_4. Volume of thin-layer cell, 5.48 μL, electrode surface area, 1.27 cm^2, temperature, T = 298 K.

to ν(C=C), ν(C=O), and ν(C-H) in-plane stretching modes. The ν(C=O) in-plane stretching at 1480 cm^{-1}, and the absence of ν(O-H) stretching at 3652 cm^{-1}, also indicate oxidation of the phenolic groups. This is similar to what was observed for hydroquinone; the H_2Q moiety is oxidatively chemisorbed to BQ on the Pd surface at all concentrations. These HREELS peaks are also utilized to determine the more likely surface orientation of the adsorbate. At the low concentration, the presence of in-plane stretch modes indicates parallel orientation with a slight tilt. This type of orientation has been confirmed by EC-STM. The images show different corrugation heights for the adsorbed BQS molecule on the surface of Pd(111) [76,77]. The image for benzoquinone sulfonic acid **(**BQS) shows dark and bright spots. The dark spot is the BQ moiety, the bright spot is an oxygen atom from the $–SO_3$ group. The tetrahedral geometry of sulfonate prevents all the oxygen atoms from being parallel to the surface, so one oxygen atom points away from the surface. This bright spot for oxygen can also be seen from the adsorbed SO_4^{2-} ions on Pd(111) and Rh by STM [28,30]. This $–SO_3$ group allows the slightly tilted flat orientation for H_2QS to occur. In contrast, the STM image of adsorbed benzoic acid on a Pt(111) surface shows the absence of surface corrugation. The planar geometry of the –COOH group does not facilitate a slightly tilted flat orientation [69]. At 3.0 mM, the surface coverage of 0.42 $nmol/cm^{-2}$ corresponds to an experimental cross-section, $\sigma_{ex,}$ of 39.3 ±0.8 $Å^2$. When comparing the value with the calculated cross-section, σ_{calc} from Figure 26, the more likely surface orientation is the 5,6-η^2.

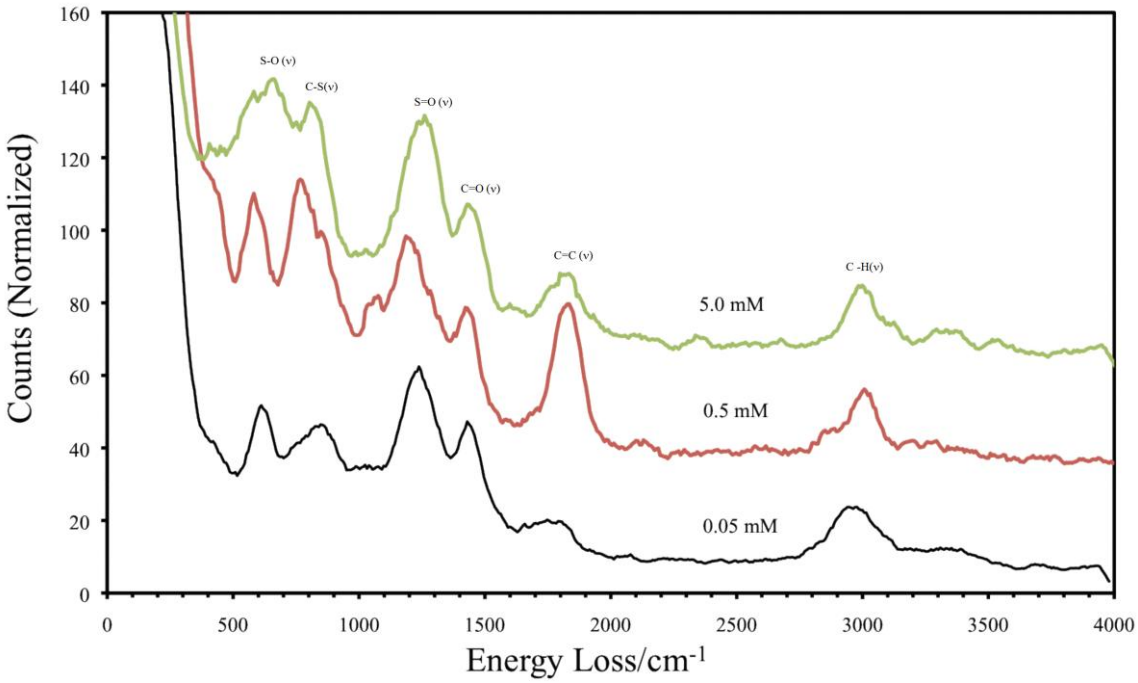

Figure 25. HREELS spectra of chemisorbed benzoquinone sulfonic acid on Pd(111) surfaces after subjecting the electrode at different concentrations of hydroquinone sulfonic acid [46].

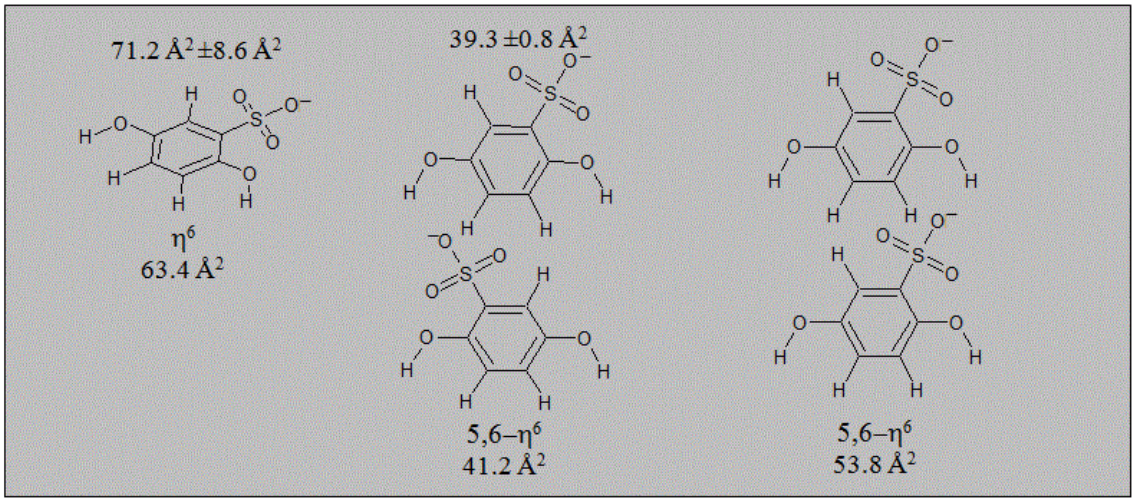

Figure 26. Mode of adsorption and calculated cross-sections of hydroquinone sulfonic acid on a metal surface.

3.4 Hydroquinone fused with aromatic rings

Figure 27 shows the chemisorption isotherm of 1,4-dihydroxynaphthalene at a smooth polycrystalline Pd electrode. Two plateaus can be clearly seen over the low and high concentrations. The plateau at low concentration also occurred in the chemisorption of TMH_2Q unlike with H_2Q, BQ, MH_2Q, and DMH_2Q. In the TMH_2Q experimental results, the presence of the methyl groups seems to allow the formation of a plateau at 0.02 mM and 0.03 mM. The benzene rings, unlike the methyl groups, have a strong affinity to metal surface, so the 1,4-dihydroxynaphthalene forms a plateau at concentrations of 0.05 mM and 0.1 mM [33,71,77]. The addition of the benzene ring to the H_2Q moiety also seems to facilitate the transition between the low concentration plateau to the high concentration as compare to the previous compounds. The three methyl groups of TMBQ also play a similar role. This Γ–plateau at low concentrations happens on polycrystalline Pt [62]. The surface coverage, Γ, of 0.22 ±0.03 corresponds to the cross-section σ_{ex} value of 74.1 ±1.1 $Å^2$. After comparing this value with all the possible σ_{calc} values corresponding to various orientations in Figure 28, the η^{10}-stucture is more likely to form on the surface, but not for 1,4-dihydroxynaphthalene [33]. In the present study, the HREELS spectra in Figure 29 show the presence of ν(C=C), ν(C=O), and ν(C-H) in-plane vibrational modes [52]. The loss peak for C=O and the absence of such for C-OH at 3500 cm^{-1} are indicative of the oxidation of H_2Q to form chemisorbed BQ regardless of the concentration. It is important to recall that in order for the loss peaks to appear at 0.05 mM, the adsorbate must have a slightly tilted flat orientation as

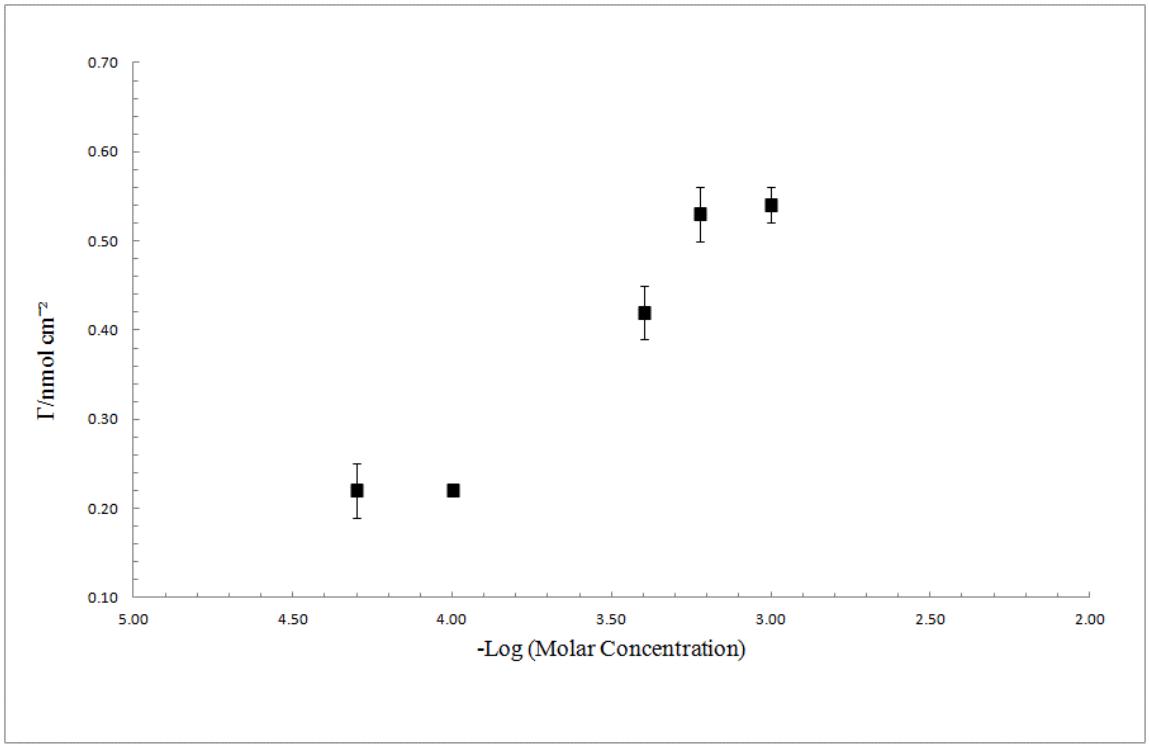

Figure 27. Chemisorption isotherm of 1,4-dihydroxynaphthalene at a smooth polycrystalline palladium electrode after subjecting the electrode to different solute concentrations. Supporting electrolyte, 1 M H_2SO_4. Volume of thin-layer cell, 5.48 μL, electrode surface area, 1.27 cm^2, temperature, T = 298 K

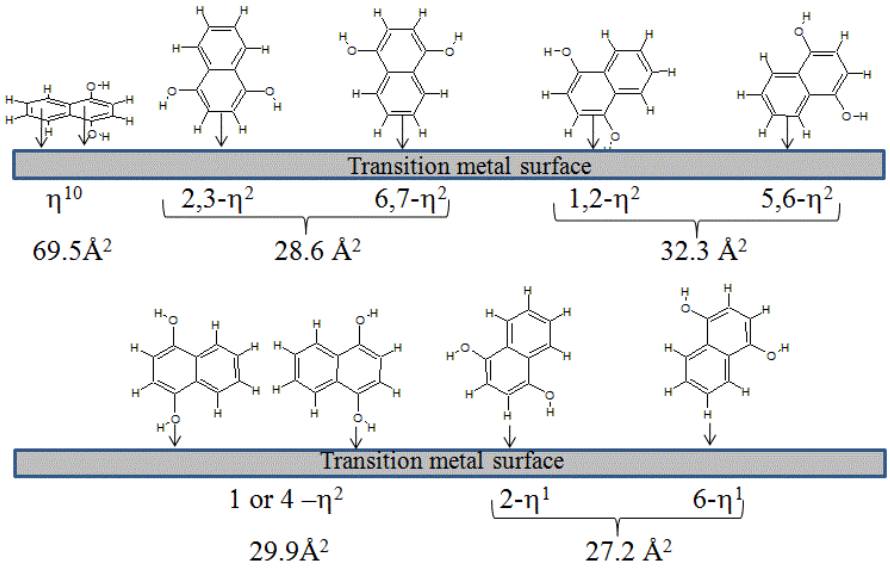

Figure 28. Mode of adsorption and calculated cross-sections of 1,4-dihydroxynaphthalene on a metal surface.

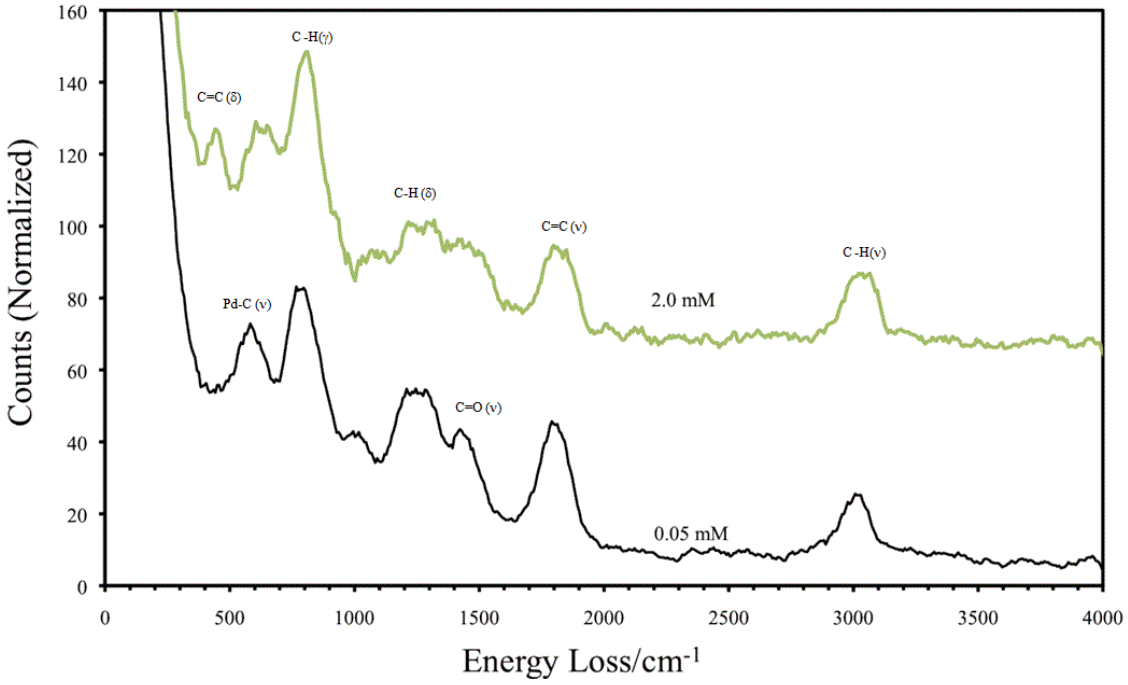

Figure 29. HREELS spectra of chemisorbed 1,4-naphthoquinone on Pd(111) surfaces after subjecting the electrode to 0.05 mM and 2.0 mM solutions of 1,4-dihydroxynaphthalene [46].

implied by the metal surface selection rule (vibration mode perpendicular to the metal surface; IR active).

At the high concentration Γ-plateau, the surface coverage of 0.54 ±0.02 nmol/cm^2 corresponds to an experimental cross-section, σ_{ex}, of 30.7 ±1.1Å^2. When comparing the σ_{ex} value to those in Figure 28, the only possible orientation is the 1 or 4-η^2-structure. Cyclic voltammetry also confirms the 1 or 4-η^2 structure as shown in Figure 30. If the 5,6-η^2, 6,7-η^2, and 6-η^1 structures are the actual orientations, the CV would have displayed reversible electroactivity peaks similar to 2,5-dihydroxythiophenol [10,42,45,78] on polycrystalline Pt. This indicates that the hydroquinone moiety is not pendant to the surface, instead it is directly bonded to the Pd surface. However, in a similar study on polycrystalline Pt, the isotherm contained two orientational transitions [62]. The σ_{ex} for the first plateau was equal to 39.5 Å^2, but the value does not correspond to any of the edgewise or endwise orientation. The explanation for the extra plateau is chemisorption with mixed orientations tilted edgewise and endwise. In contrast, the chemisorption of 1,4-dihydroxynaphthalene results only in orientations shown in Figure 28.

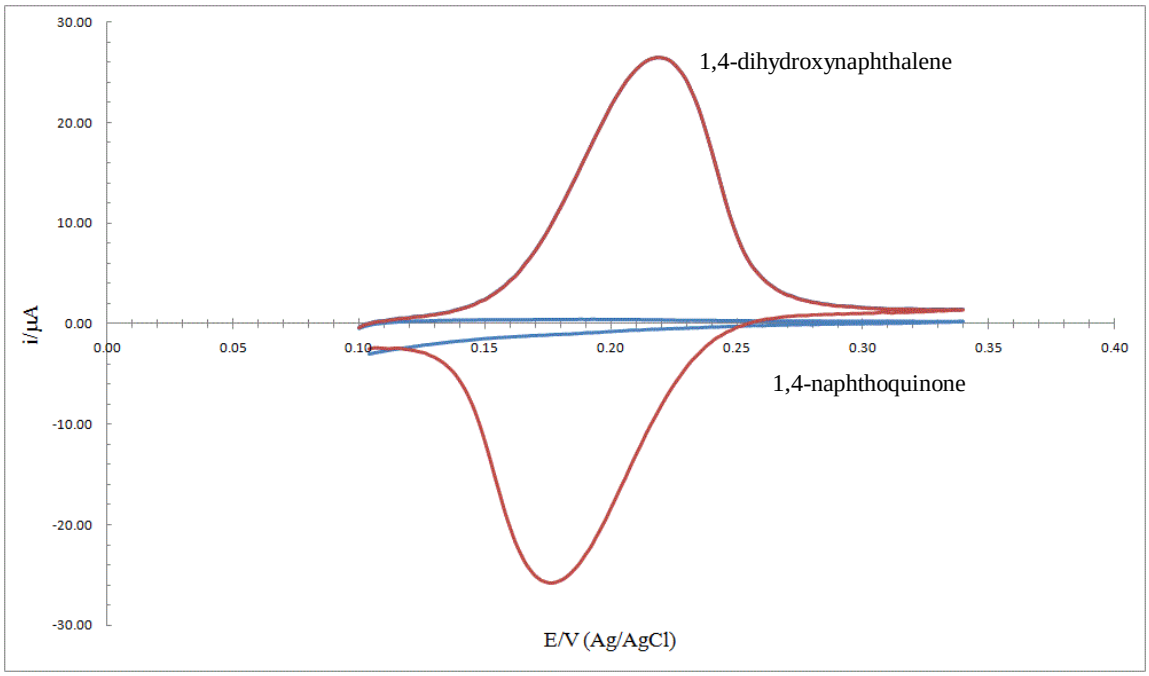

Figure 30. Cyclic voltammograms of unadsorbed 1,4-dihydroxynaphthalene (1.0 mM) and adsorbed 1,4-naphthoquinone in 1.0 M H_2SO_4.. Scan rate, 2 mV/s.

3.5 Hydroquinone substituted with a phenyl group

Figure 31 shows the chemisorption isotherm of phenylhydroquinone after exposing the polycrystalline Pd electrode to various solution concentrations. The isotherm is similar to the result for polycrystalline Pt except at the low concentration regime. On Pt, a Γ-plateau exists between 0.03 mM and 0.01 mM, while the Γ-plateau on Pd is non-existing [62]. In order to determine the experimental cross-section (σ_{ex}), the lowest surface coverage of 0.19 ±0.03 nmol/cm^2 was used. The value of 0.19 ±0.03 nmol/cm^2 corresponds to 88.3 ±12.1 Å^2. Even with a high cross-section error, the value is closer to the calculated cross-section, σ_{cal}, of 85.1 Å^2 of the η^6-structure as shown in Figure 32.

Figure 33 shows the HREELS spectra of phenylbenzoquinone after exposing the Pd(111) surface to 0.05 mM, 0.5 mM, and 5.0 mM of phenylhydroquinone solutions. The spectra show the absence of the ν(O-H) in-plane stretching peak at 3500 cm^{-1} and the presence of the ν(C=O) in-plane vibrational mode at 2862 cm^{-1} [52]. The phenylhydroquinone is oxidized to form phenylbenzoquinone as in the previous hydroquinone derivatives. This surface activity is independent of the adsorbate concentration. As implied by the surface-metal selection rule for IR-active vibrational modes, the presence of the ν(C=C), ν(C=O), and ν(C-H) in-plane modes indicate a slightly tilted flat orientation [1,19].

As the concentration increases from 0.03 mM to 0.3 mM, the surface coverage increases until forming a Γ-plateau between 0.3 mM and 0.8 mM as shown in Figure 31.

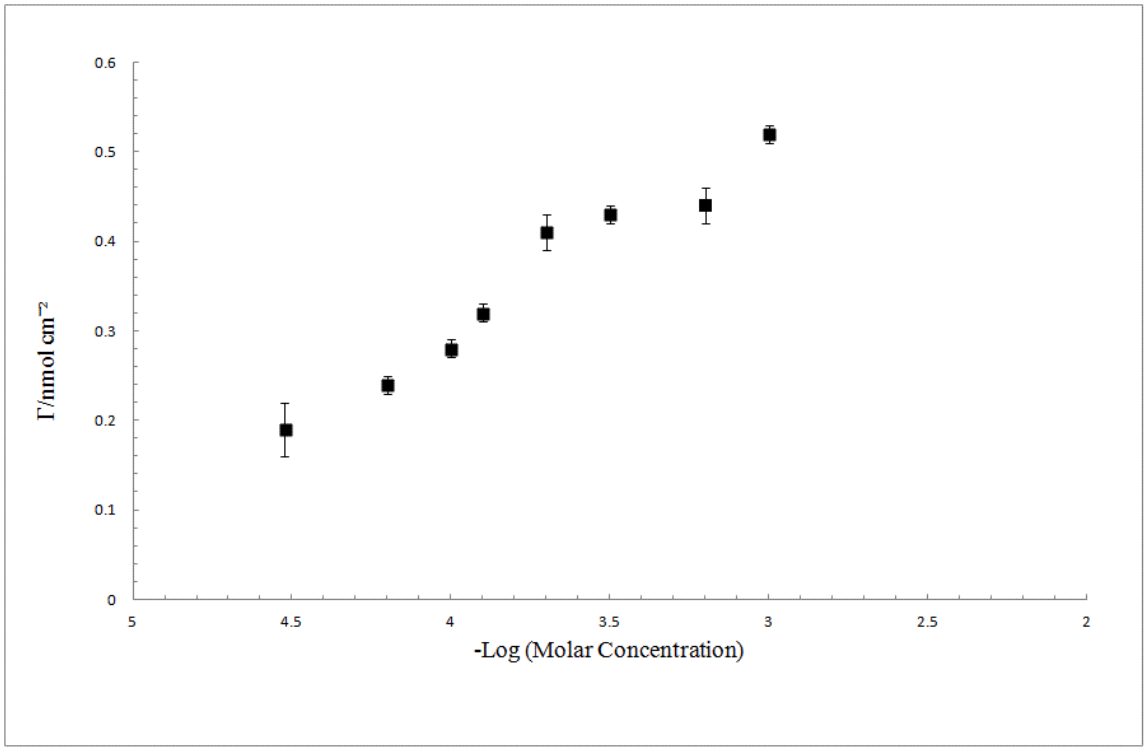

Figure 31. Chemisorption isotherm of phenylhydroquinone at a smooth polycrystalline palladium electrode after subjecting the electrode to different solute concentrations. Supporting electrolyte, 1 M H_2SO_4. Volume of thin-layer cell, 5.48 μL, electrode surface area, 1.27 cm^2, temperature, T = 298K.

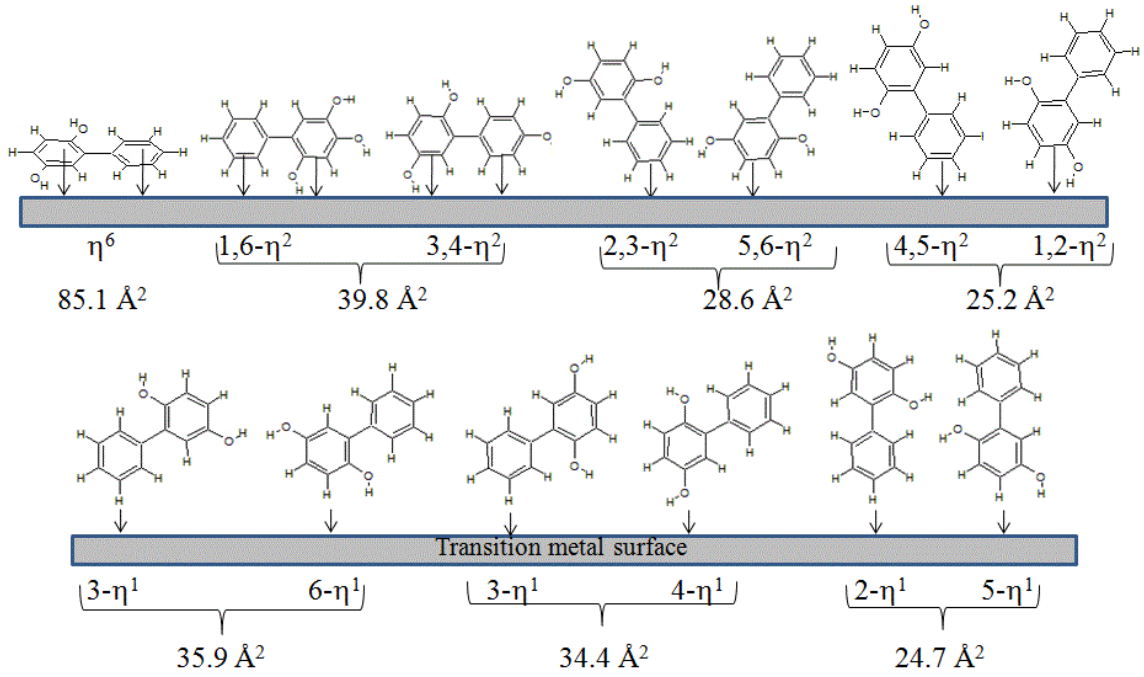

Figure 32. Mode of adsorption and calculated cross-sections of phenylhydroquinone on a metal surface.

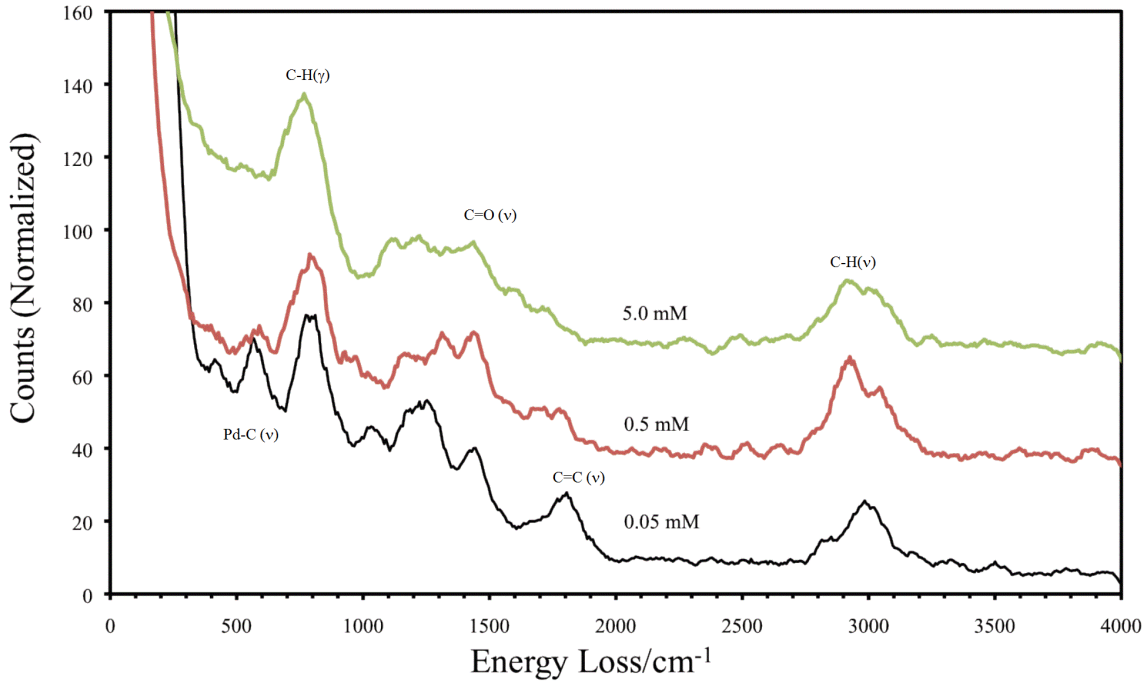

Figure 33. HREELS spectra of chemisorbed phenylbenzoquinone on Pd(111) surfaces after subjecting the electrode to 0.05 mM, 0.5 mM, and 5.0 mM solution of phenylhydroquinone [52].

The surface coverages of 0.43 ±0.01 nmol/cm^2 and 0.43 ±0.02 nmol/cm^2 correspond to experimental cross-sections, $\sigma_{ex,}$ of 37.6 ±1.7 Å^2 and 37.8 ±1.0 Å^2, respectively. Figure 32 shows the orientations and the calculated cross-sections of phenylquinone on a metal surface. A comparison between experimental and calculated cross-sections reveals that both σ_{ex} are very close to the calculated cross-section, $\sigma_{cal,}$ of 39.8 Å^2. The η4-structure (1,6,3,4-η^4 and 2,3,5,6-η^4) is similar to the edge-wise structure on polycrystalline Pt [62].

At 1.0 mM, the surface coverage cross-section, Γ, of 0.52 ±0.04 Å^2 corresponds to an experimental cross-section, $\sigma_{ex,}$ of 32.1 ±0.4 Å^2. The σ_{ex} is much closer to the calculated cross-section, $\sigma_{cal,}$ of 28.6 Å^2, compared to the other calculated cross-sections. The phenylhydroquinone prefers a η^2-structure with one aromatic ring pendant to the surface. The HREELS and cyclic voltammetry were used to determine the type of aromatic ring (hydroquinone or phenyl moiety) chemisorbed on the surface. The HREELS spectrum for 5.0 mM shows the absence of the O-H stretching mode at 3500 cm^{-1}. The absence of the O-H peak can only occur when the hydroquinone moiety is oxidatively chemisorbed to the Pd surface. Cyclic voltammetry also confirms the 5,6-η^2 orientation by the lack of electroactivity of the hydroquinone moiety as shown in Figure 34. In contrast, the figure on page 89 shows the cyclic voltammogram of the oxidation and reduction peaks of chemisorbed of 2,5-dihydroxythiophenol. The anodic and cathodic peaks indicate electroactivity of the pendant hydroquinone moiety.

In a similar study on smooth polycrystalline Pt, the chemisorbed phenylhydroquinone molecule, however, showed a small reversible

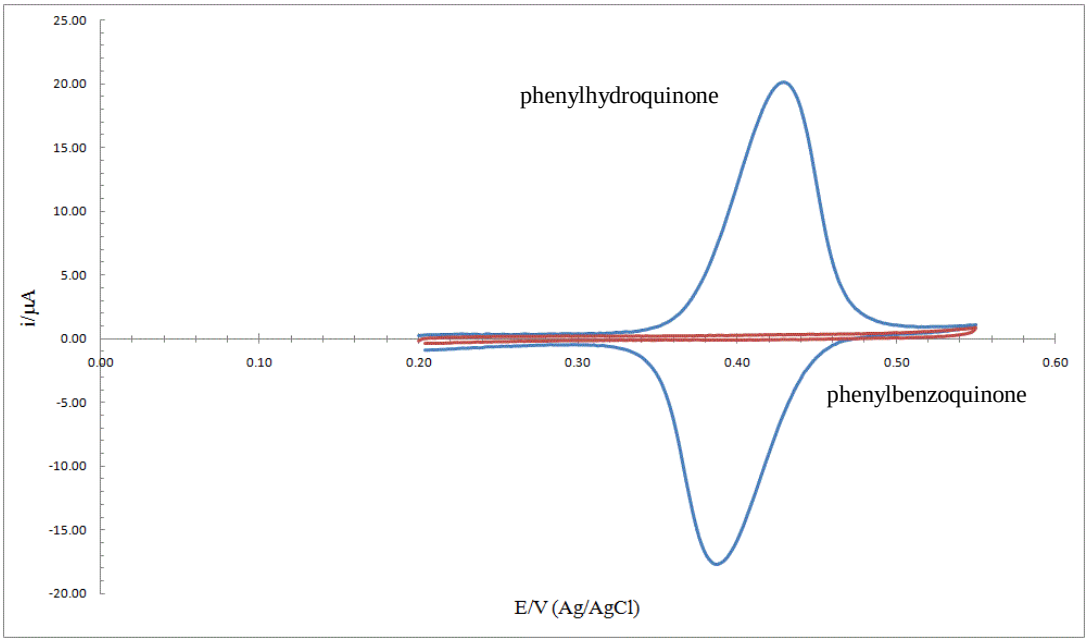

Figure 34. Cyclic voltammogram of unadsorbed (1.0 mM) phenylhydroquinone and adsorbed phenylbenzoquinone in 1.0 M H_2SO_4. Scan rate, 2 mV/s.

electroactivity [62,79]. The extent of the electroactivity was determined to be 17% of the adsorbate. This activity is possible when some benzene moieties are attached to the Pd surface instead of the hydroquinone moiety. However, both results from HREELS and cyclic voltammetry are in agreement that the hydroquinone moiety does not show electroactivity on the Pd surface.

3.6 Heteroaromatic

The presence of nitrogen in 2,3-dihydroxypyridine offers an additional metal-ligand bond with the surface besides the metal-olefin and metal-C bonds. Since 2,3-dihydroxypyridine is a weak base, the extent of nitrogen-metal interaction is pH dependent. At pH 0, the electron lone pair of the heteroatom in the aromatic ring becomes protonated, and N-coordination with the metal surface is then inhibited. At pH 7, the electron lone pair is free from protonation and thus, the interaction between the heteroatom and the metal surface is possible. Figure 35 shows the chemisorption isotherm of 2,3-dihydroxypyridine on a smooth polycrystalline palladium electrode in 1 M H_2SO_4. Since the 2,3-dihydroxypyridine isotherm lacks a Γ–plateau at low concentrations unlike on polycrystalline Pt, the lowest surface coverage, Γ, of 0.19 ±0.01 nmol/cm^{-1} was used to determine the experimental cross-section, σ_{ex} [62]. The σ_{ex} of 88.1 ±4.0 Å^2 is larger than the calculated cross-section (54.4 Å^2) as illustrated in Figure 36. It seems that the presence of the protonated nitrogen atom lowers the affinity of 2,3-dihydroxypyridine to the Pd surface.

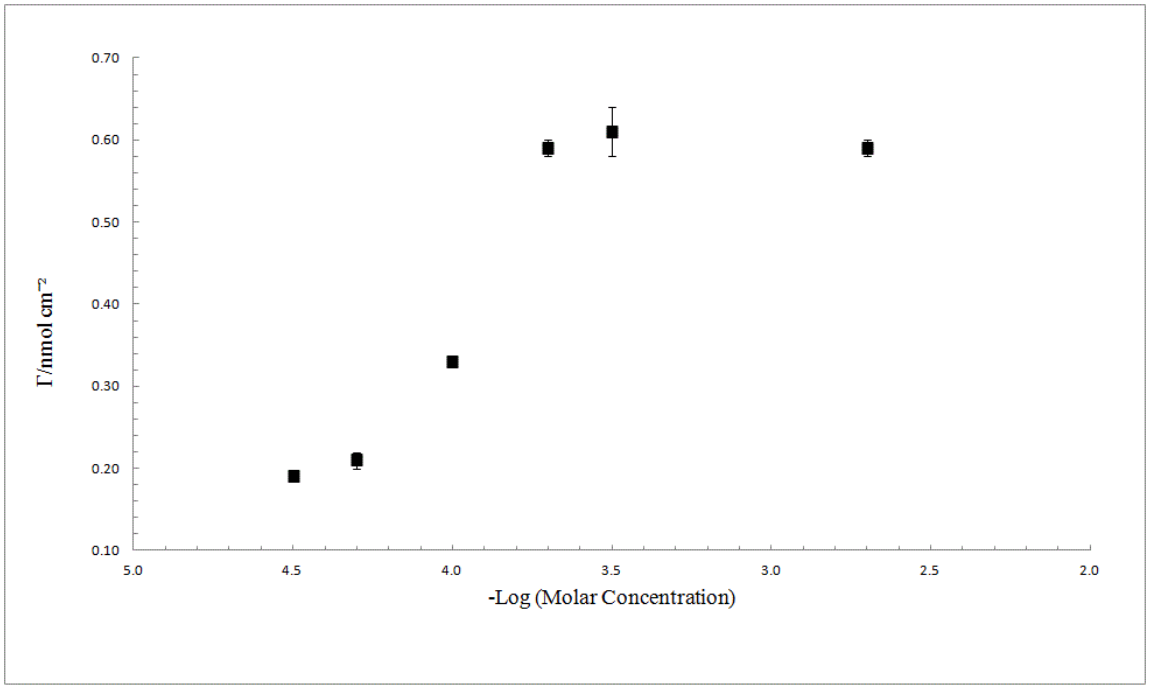

Figure 35. Chemisorption isotherm of 2,3-dihydroxypyridine at a smooth polycrystalline palladium electrode after subjecting the electrode to different solute concentrations. Supporting electrolyte, 1 M H_2SO_4. Volume of thin-layer cell, 5.48 μL, electrode surface area, 1.27 cm^2, temperature, T = 298.

The low surface affinity is similar to pyridine on Au(111) [80]. Even though the surface coverage had a value of 0.14 nmol/cm^2, the STM image showed a flat-orientated pyridine. The η^6-orientation was also confirmed by Osawa et al 1998. In both studies, the pyridine orientation was pH independent. Since the nitrogen heteroatom at pH 0 becomes protonated, which prevents a η^1-N coordination, the coordination modes can only occur by the hydroquinone moiety. In this study, the HREELS spectrum confirms the protonation of nitrogen as shown in Figure 36. As per the metal surface selection rule, the vibrational modes are only HREELS-active if the adsorbate has a slightly tilted flat orientation. Even though 2,3-dihydroxypyridine has a low affinity to Pd, the adsorbate probably has a flat orientation with a slight tilt with a coordination via the π electrons of the aromatic ring. Likewise, for 2,3-dihydroxypyridine on polycrystalline Pt electrodes, the surface coverage of 0.45 nmol/cm^2 corresponds to an experimental cross-section, $\sigma_{ex,}$ of 39.1±1.4 Å^2, but the σ_{ex} also does not correlate to any of the calculated cross-sections [62].

As the concentration increases from 0.05 mM, the transition between the lower and upper plateaus is more abrupt for 2,3-dihydroxypyridine than H_2Q as shown in Figure 35 and Figure 13. The presence of the heteroatom in the aromatic ring seems to facilitate the chemisorption, compared to H_2Q on the Pd surface. This behavior is similar to 3,6-dihydroxypyridazine [81]. At high concentrations, the Γ-plateau has a value of 0.59 ±0.01 nmol/cm^{-2}, which corresponds to the experimental the cross -section of 28.1 ±0.7 A^2. In comparison with all the calculated cross-sections, σ_{cal}, 28.1 ±0.7 A^2 is closer to 26.9 Å^2 for a η^2-orientation as shown in Figure 37. The mode of adsorption has

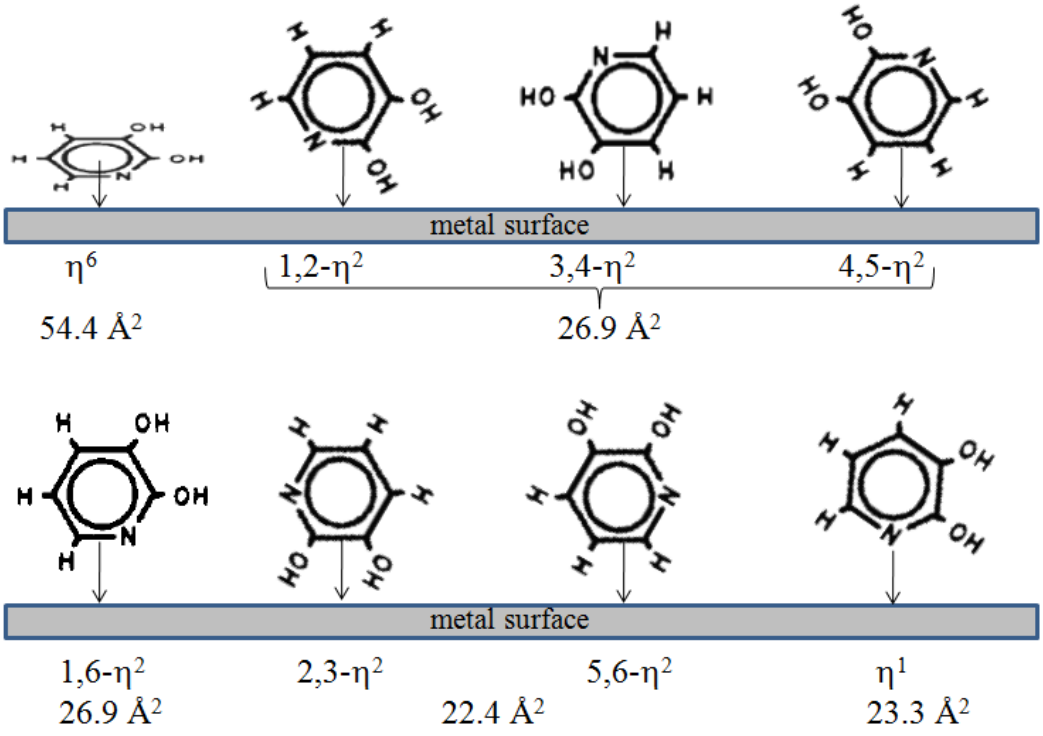

Figure 36. Mode of adsorption and calculated cross-sections of 2,3-dihydroxypyridine on a metal surface.

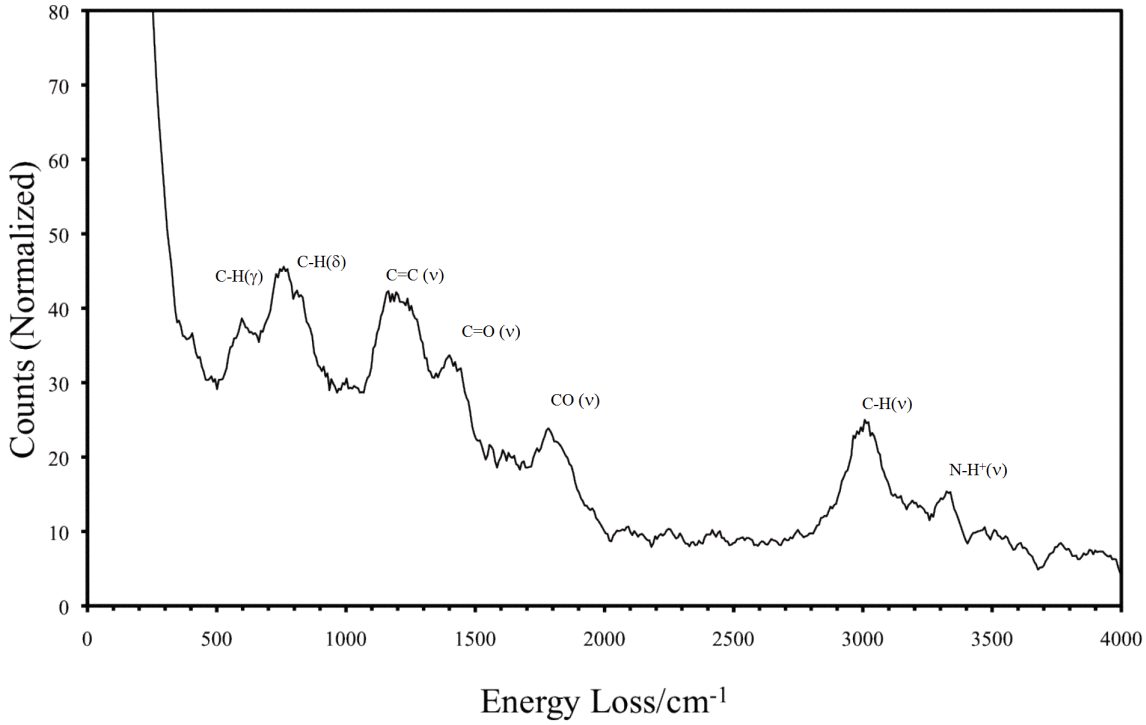

Figure 37. HREELS spectra of chemisorbed of 2,3-dihydroxypyridine on Pd(111) surfaces after subjecting the electrode to 0.05 mM solution at pH 2 [46].

several structures (1,2-η^2, 3,4-η^2, 4,5-η^2, and 1,6-η^2) for this calculated cross-section. Even though the HREELS spectrum shows the presence of ν(O-H) stretching at 3300 cm^{-1} at 0.05 mM for the 2,3-dihydroxypyridine solution, it is possible that the O-H stretching also occurs at higher concentrations. Therefore, all the 1,2-η^2, 3,4-η^2, 4,5-η^2, and 1,6-η^2 structures, or a mixture of structures, are possible.

3.7 Hydroquinone substituted with mercapto groups

Figure 38 shows the cyclic voltammograms of chemisorbed 2,5-dihydroxythiophenol (DHT) at 0.02 mM and 2.0 mM. At a low concentration, the two-electron and two proton redox reactions for hydroquinone (H_2Q) to benzoquinone (BQ) are non-existing. The lack of electroactivity indicates the adsorbate to be parallel to the Pd surface. This structure is not surprising because the sulfur atom, like the H_2Q moiety, also has an affinity to metal surfaces [41,52,59,78,82]. This result is almost identical to that on a polycrystalline Ir electrode except that the reversible electroactivity of the diphenol/quinone couple is barely noticeable [59,78]. However, the reversible electroactivity is more profound on polycrystalline Pt and Au electrodes [45,83,84]. Since the H_2Q moiety has no affinity towards the Au surface, the H_2Q group becomes pendant through the sulfur atom. This η^1-structure allows the redox activity to occur.

Figure 39 shows the HREELS spectrum of chemisorption DHT on Pd(111) after exposure to a 0.02 mM solution. Overall, the HREELS spectrum in Figure 40 is similar to the other hydroquinone derivatives. The spectra shows the absence of the ν(O- H)

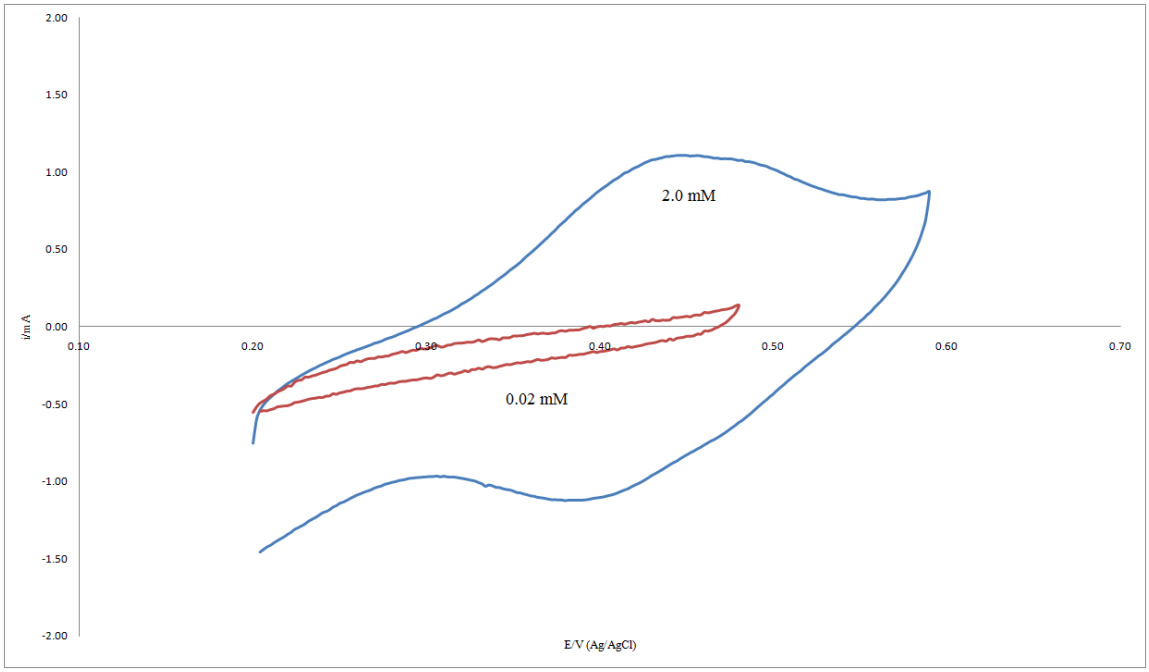

Figure 38. Cyclic voltammograms of DHT after several aliquots of 0.02 mM and 2.0 mM solutions recorded in 1.0 M H_2SO_4. Scan rate, 2 mV/s.

in-plane stretching at 3500 cm^{-1} and the presence of the ν(C=O) in-plane vibrational mode at 1480 cm^{-1} [52]. The spectrum also shows the absence of the S-H peak at 2500 cm^{-1}. This result indicates the loss of the mercaptan hydrogen during chemisorption [11]. This type of chemisorption also occurs for the chemisorption of DHT on Ir [59,78]. Therefore, the adsorption of DHT on polycrystalline Pd is the simultaneous surface coordination of the sulfur and aromatic ring [85]. This type of bonding refers to surface chelation as a η^7-structure. The chemisorption of DHT can be represented by the equation:

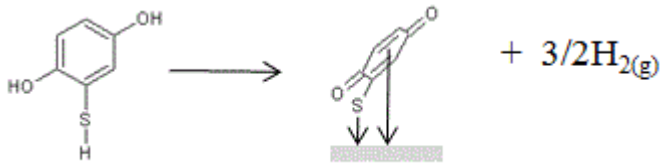

(45)

Figure 38 also shows the cyclic voltammogram of chemisorbed DHT on polycrystalline Pd after exposing the Pd electrode to a 2.0 mM solution of the compound. It shows the presence of the reversible electroactivity of the diphenol/quinone couple. The redox activity is only possible when the sulfur atom has a surface coordination with Pd. The higher concentration of DHT favors the oxidative chemisorption of the thiophenol moiety, unlike chemisorption of the phenolic groups from the DHT at low concentrations.

Figure 40 shows the HREELS spectra of chemisorbed DHT on a Pd(111) electrode after subjecting the electrode to a 0.25 mM solution at 0.05 V (a), and after

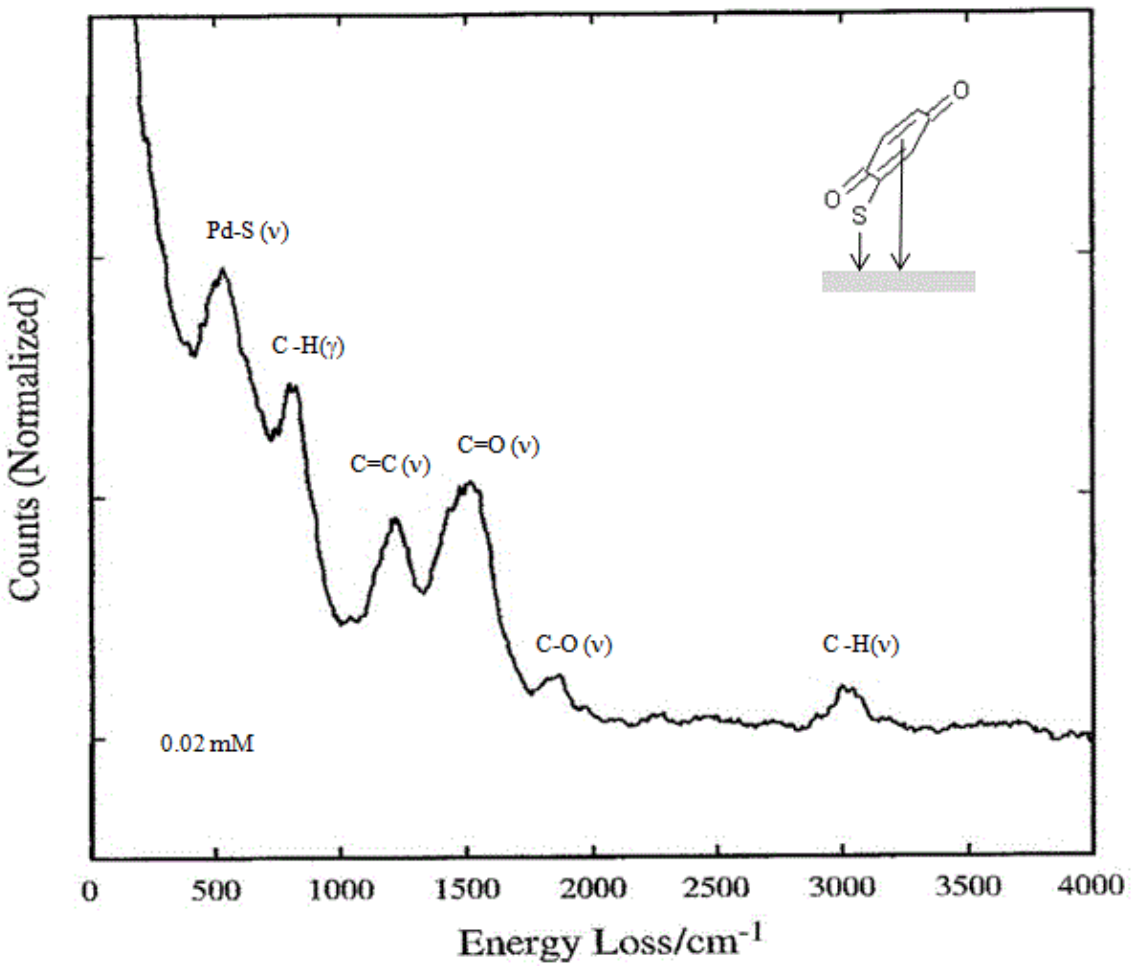

Figure 39. HREELS spectrum of chemisorbed dihydroxythiophenol on Pd(111) surfaces after subjecting the electrode to a 0.02 mM solution at pH 2 [46].

applying 0.5 V (b). The absence of a peak from the S-H stretch at 2590 cm^{-1} indicates oxidative chemisorption of the S-H group [86,87]. The spectrum also shows the presence of the in-plane mode, ν(O-H), at 3544 cm^{-1} when 0.05 V was applied to the Pd(111) electrode. Since 0.5 V was applied after chemisorption to produce benzoquinone, the oxidation of the phenolic groups is dependent on the interaction between the H_2Q moiety and the Pd surface.

Since the cathodic peak was not well defined, as shown in Figure 38, the area under the anodic peak (charge) was used to determine the surface coverage, Γ. The Γ ($0.61 nmol/cm^2$) represents an experimental cross-section, $\sigma_{ex,}$ of 27.2 $Å^2$. This cross-section is closer to the calculated cross-section, $\sigma_{calc,}$ of 28.6 $Å^2$ of H_2Q. A closer look at the cyclic voltammetry for the redox peaks of DHT clearly shows peak broadening for the anodic peak and the semi-reversible cathodic peak. The electrochemical process is not limited to polycrystalline Pd. The same broadening of the anodic peaks can also be ound on polycrystalline Pt and Ir [41,45,50,59,83,84]. Since broadening of the anodic and cathodic peaks for the polycrystalline Au electrode does not occur, the proximity of the adsorbate molecules does not induce peak broadening [79,80]. The interaction might produce the presence of a quinhydrone complex. This complex is known to be highly stable in a 1:1 quinone to diphenol ratio within the adsorbed DHT. As mentioned in the introduction, the quinone/diphenol reaction, therefore, is substrate-mediated and not mediated by adsorbate-adsorbate interactions through space between the pendent f hydroquinone moieties [79,80]. The quinone/diphenol couple is illustrated as follows [32]:

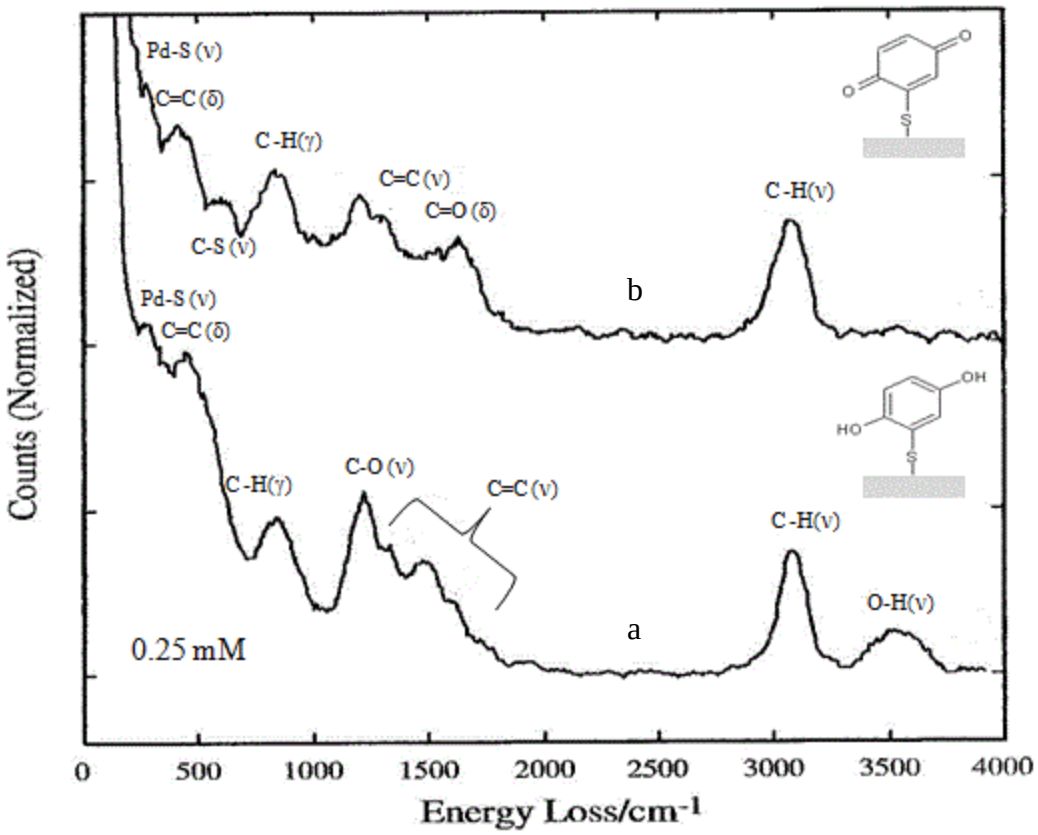

Figure 40. HREEL spectra of chemisorbed DHT on Pd(111)) surfaces after subjecting the Pd electrode to a 0.25 mM solution of DHT at 0.05 V (a) and after applying 0.5 V (b) [85].

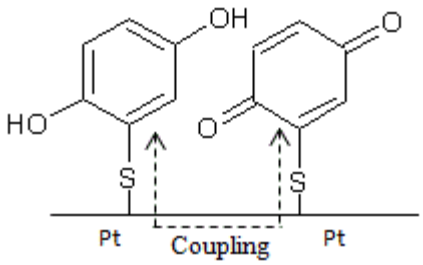

(46)

2-(8-mecaptooctyl)-1,4-benzenediol (DHOT) with an alkyl chain between the –SH and H_2Q moiety can provide further information on the substrate-mediated adsorbate-adsorbate interactions. Figure 41 shows the cyclic voltammogram of DHOT on polycrystalline Pd. The redox peaks of DHOT are more defined than DHT (Figure 38). The addition of an 8-carbon alkyl chain seems to disrupt the adsorbate-adsorbate interactions through the metal (surface-mediated). This electrochemical reactivity is not surprising because the addition of one $–CH_2-$ "insulator" group between the sulfur and the hydroquinone moiety has shown to block the surface-mediated interactions on Pt and Ir electrodes [41]. This surface disruption explains the difference in full width at half maximum (FWHM) of the voltammetric peak of 0.35 V for DHOT compared to 0.44 V for DHT. The redox activity ferrocene group of ($Fc(CH_2)_nSH$) also occurred from a 9 and 11 carbon alkyl chain chemisorbed on Au(111) surface [88].

DHOT seems to have similar adsorption properties as DHT at 0.02 mM. In the first four aliquots of using the 0.04 mM solution, the cyclic voltammograms showed the absence of the redox activity of the H_2Q moiety. These results indicate that both, the sulfur atom and the H_2Q moiety, are chemisorbed on the Pd surface. In Figure 42, the HREELS spectrum confirms the absence of the –S-H bend at 2590 cm^{-1} and the –OH

vibrational mode at 3500 cm^{-1}. The spectrum does show the presence of the ν(C=O) and ν(C-H) stretching. The long alkyl chain seems not to hinder the oxidation of the phenolic group. However, the presence of the 8-carbon alkyl chain prevents a strong interaction between the aromatic ring and the Pd surface. As the Pd electrode is exposed to several aliquots of 0.04 mM DHOT, redox peaks appear as shown in Figure 42. The sulfur atoms with higher affinity to the surface tend to displace H_2Q. This type of surface reaction is called ligand exchange. Since chemisorbed H_2Q is redox inert, the redox activity can only occur by a pendant H_2Q. The surface coverage of 0.535 $nmol/cm^2$ corresponds to the experimental cross-section σ_{ex} of 31.3 $Å^2$. The σ_{ex} is closer to the calculated cross-section of 28.6 $Å^2$ for H_2Q.

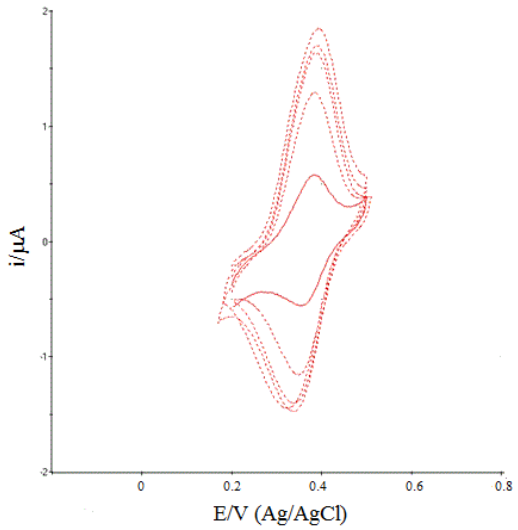

Figure 41. Cyclic voltammogram of DHOT after multiple aliquots of 0.04 mM solutions recorded in supporting electrolyte, 1 M H_2SO_4. Scan rate, 2 mV/s.

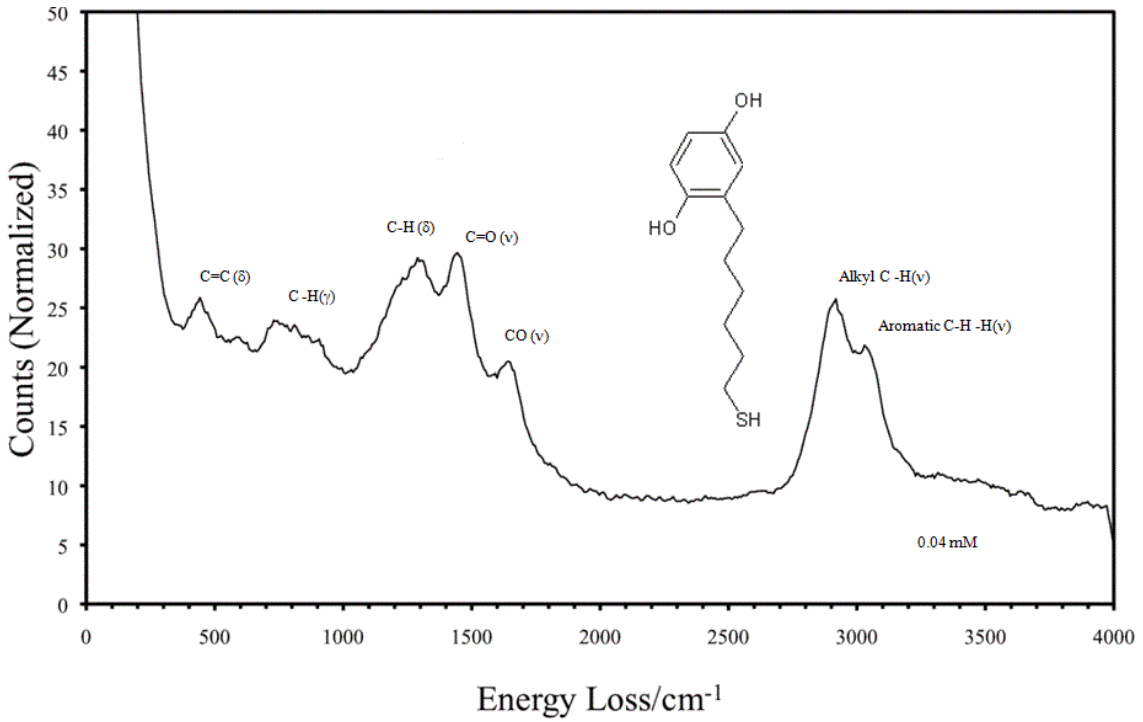

Figure 42. HREELS spectrum of chemisorbed DHOT on single crystal Pd(111) surface after subjecting the electrode to a 0.04 mM solution of DHOT [52].

4. CONCLUSIONS

The studies of the resulting organic compounds by thin-layer electrochemistry and high-resolution electron energy spectroscopy revealed several trends for the surface coverage, orientation, and mode of attachment as function of concentration on Pd electrodes. The current findings may serve as a guide for future studies of the interaction of aromatic compounds on other transition metals other than Pt or Pd. The experimental results show the following trends for the selected aromatic compounds:

1. Diphenolic compounds are oxidatively chemisorbed as quinones on polycrystalline Pd electrodes.
2. At a low solute concentration ($C < 0.1$ mM), the chemisorbed homoaromatics adopt essentially flat orientations.
3. At a high solute concentration ($C > 0.1$ mM), the chemisorbed homoaromatics adopt vertical (most probably edge-wise) orientations.
4. Competitive chemisorption occurs between the surface-active functional groups (-N and -SH) and the aromatic moiety.
5. The preferential chemisorption of the subject compounds to the Pd electrode increases in the order: phenyl ring < quinone ring << -SH.

REFERENCES

[1] E. McCash, M., Surface Chemistry, Oxford University Press, Oxford, UK, 2001.

[2] G. A. Somorjai, Introduction to Surface Chemistry and Catalysis, John Wiley, New York, 1994.

[3] R. Akiyama, S. Kobayashi, J Am Chem Soc 125 (2003) 3412-3413.

[4] K. P. Peterson, R. C. Larock, The Journal of Organic Chemistry 63 (1998) 3185-3189.

[5] H. Gao, R. J. Angelici, J Am Chem Soc 119 (1997) 6937-6938.

[6] Yin, J. Liebscher, Chem Rev 107 (2006) 133-173.

[7] K. Mori, K. Yamaguchi, T. Hara, T. Mizugaki, K. Ebitani, K. Kaneda, J Am Chem Soc 124 (2002) 11572-11573.

[8] W. Huang, J. H.-C. Liu, P. Alayoglu, Y. Li, C. A. Witham, C.-K. Tsung, F. D. Toste, G. A. Somorjai, J Am Chem Soc 132 (2010) 16771-16773.

[9] N. I. Il'chenko, G. I. Golodets, Journal of Catalysis 39 (1975) 57-72.

[10] D. A. Stern, L. Laguren-Davidson, D. G. Frank, J. Y. Gui, C. H. Lin, F. Lu, G. N. Salaita, N. Walton, D. C. Zapien, A. T. Hubbard, J Am Chem Soc 111 (1989) 877-891.

[11] D. A. Stern, E. Wellner, G. N. Salaita, L. Laguren-Davidson, F. Lu, N. Batina, D. G. Frank, D. C. Zapien, N. Walton, A. T. Hubbard, J Am Chem Soc 110 (1988) 4885-4893.

[12] S. A. Chaffins, J. Y. Gui, C. H. Lin, F. Lu, G. N. Salaita, D. A. Stern, A. T. Hubbard, Langmuir 6 (1990) 1273-1281.

[13] J. Y. Gui, B. E. Kahn, L. Laguren-Davidson, C. H. Lin, F. Lu, G. N. Salaita, D. A. Stern, A. T. Hubbard, Langmuir 5 (1989) 819-828.

[14] F. Lu, G. N. Salaita, L. Laguren-Davidson, D. A. Stern, E. Wellner, D. G. Frank, N. Batina, D. C. Zapien, N. Walton, A. T. Hubbard, Langmuir 4 (1988) 637-646.

[15] J. L. Stickney, S. D. Rosasco, D. Song, M. P. Soriaga, A. T. Hubbard, Surf Sci 130 (1983) 326-347.

[16] F. R. Hartley, Chemistry of Platinum and Palladium, John Wiley & Sons, New York, 1973.

[17] J. Sanabria-Chinchilla, J. H. Baricuatro, M. P. Soriaga, F. Hernandez, H. Baltruschat, J Colloid Interf Sci 314 (2007) 152-159.

[18] C. Morin, D. Simon, P. Sautet, The Journal of Physical Chemistry B 108 (2004) 5653-5665.

[19] K. Kolasinski, W., Surface Sience Foundations of Catalysis and Nanoscience, John Wiley & Sons, LTD, West Sussex, England, 2002.

[20] A. Wieckowski, Interfacial Electrochemistry, Marcel Dekker, Inc, New York, 1999.

[21] M. D. Lay, K. Varazo, J. L. Stickney, Langmuir 19 (2003) 8416-8427.

[22] E. Ross Montgomery, R. W. Murray, Analytica Chimica Acta 321 (1996) 195-199.

[23] L. R. F. Allen J. Bard, Electrochemical Methods Fundamentals and Applications, John Wiley & Sons, Inc., New York, 2001.

[24] K. Sashikata, Y. Matsui, K. Itaya, M. P. Soriaga, J Phys Chem-Us 100 (1996) 20027-20034.

[25] A. Carrasquillo, J. J. Jeng, R. J. Barriga, W. F. Temesghen, M. P. Soriaga, Inorg Chim Acta 255 (1997) 249-254.

[26] D. F. Shriver, Inorganic Chemistry, 3rd ed., Oxford University Press, Oxford, UK, 1999.

[27] F. A. Cotton, Basic Inorganic, 3rd ed., John Wiley & Sons, Inc, New York, 1995.

[28] L.-J. Wan, S.-L. Yau, K. Itaya, The Journal of Physical Chemistry 99 (1995) 9507-9513.

[29] A. J. Bard, H. D. Abruna, C. E. Chidsey, L. R. Faulkner, S. W. Feldberg, K. Itaya, M. Majda, O. Melroy, R. W. Murray, M. D. Porter, M. P. Soriaga, H. S. White, J Phys Chem-Us 97 (1993) 7147-7173.

[30] Y. G. Kim, J. B. Soriaga, G. Vigh, M. P. Soriaga, J Colloid Interf Sci 227 (2000) 505-509.

[31] M. P. Soriaga, J. H. White, D. Song, A. T. Hubbard, J Phys Chem-Us 88 (1984) 2284-2287.

[32] M. P. Soriaga, Chem Rev 90 (1990) 771-793.

[33] S.-L. Yau, Y.-G. Kim, K. Itaya, The Journal of Physical Chemistry B 101 (1997) 3547-3553.

[34] S.-L. Yau, Y.-G. Kim, K. Itaya, J Am Chem Soc 118 (1996) 7795-7803.

[35] K. Sashikata, T. Sugata, M. Sugimasa, K. Itaya, Langmuir 14 (1998) 2896-2902.

[36] T. Shimooka, S. Yoshimoto, M. Wakisaka, J. Inukai, K. Itaya, Langmuir 17 (2001) 6380-6385.

[37] K. Suto, M. Wakisaka, M. Yamagishi, L. J. Wan, J. Inukai, K. Itaya, Langmuir 16 (2000) 9368-9373.

[38] M. Wakisaka, K. Suto, J. Inukai, K. Itaya, Langmuir 18 (2002) 729-733.

[39] Y.-C. Yang, Y.-P. Yen, L.-Y. Ou Yang, S.-L. Yau, K. Itaya, Langmuir 20 (2004) 10030-10037.

[40] M. P. Soriaga, E. Binamirasoriaga, A. T. Hubbard, J. B. Benziger, K. W. P. Pang, Inorg Chem 24 (1985) 65-73.

[41] M. E. Bothwell, M. P. Soriaga, Journal of Electroanalytical Chemistry and Interfacial Electrochemistry 295 (1990) 123-138.

[42] B. G. Bravo, S. L. Michelhaugh, M. P. Soriaga, J Electroanal Chem 241 (1988) 199-210.

[43] C. Creutz, Progress Inorganic Chemistry 1 (1983).

[44] P. C. Ford, D. P. Rudd, R. Gaunder, H. Taube, J Am Chem Soc 90 (1968) 1187-1194.

[45] B. G. Bravo, T. Mebrahtu, M. P. Soriaga, D. C. Zapien, A. T. Hubbard, J. L. Stickney, Langmuir 3 (1987) 595-597.

[46] X. L. Chen, J. Sanabria-Chinchilla, M. P. Soriaga, Electroanal 17 (2005) 2121-2127.

[47] X. Chen, Ph.D. dissertation, Texas A&M University College Station, 2004.

[48] J. Sanabria-Chinchilla, Ph.D. dissertation, Texas A&M University, College Station 2006.

[49] Y. P. Gui, T. Kuwana, Langmuir 2 (1986) 471-476.

[50] T. Mebrahtu, G. M. Berry, M. P. Soriaga, J Electroanal Chem 239 (1988) 375-386.

[51] K. L. Vieira, D. C. Zapien, M. P. Soriaga, A. T. Hubbard, K. P. Low, S. E. Anderson, Anal Chem 58 (1986) 2964-2968.

[52] D. LI, Texas A&M Universtiy, College Station 2010.

[53] F. J. H. Timothy A. Nieman, Douglas A. Skoog, Principles of Instrumental Analysis, 5th ed., Saunders College Publishing, Philadelphia, 1998.

[54] J. Wang, Analytical Electrochemistry, Third ed., John Wiley & Sons, Inc., Hoboken, New Jersey, 2006.

[55] K. Itaya, S. Sugawara, K. Sashikata, N. J. Furuya, Vac. Sci. Technol. A8 (1990) 515.

[56] M. P. Soriaga, A. T. Hubbard, J Am Chem Soc 104 (1982) 2735-2742.

[57] L. C. Pauling, The Nature of the Chemical Bond, 3rd ed. ed., Cornell University Press, Ithaca, New York, 1960.

[58] A. T. Hubbard, V. K. F. Chia, M. P. Soriaga, J. H. White, J Electrochem Soc 133 (1986) C127-C127.

[59] M. E. Bothwell, J. F. Rodriguez, M. P. Soriaga, Journal of Electroanalytical Chemistry and Interfacial Electrochemistry 252 (1988) 453-459.

[60] A. T. Hubbard, Chem Rev 88 (1988) 633-656.

[61] M. P. Soriaga, A. T. Hubbard, J Am Chem Soc 104 (1982) 2742-2747.

[62] M. P. Soriaga, A. T. Hubbard, J Am Chem Soc 104 (1982) 3937-3945.

[63] M. P. Soriaga, P. H. Wilson, A. T. Hubbard, C. S. Benton, J Electroanal Chem 142 (1982) 317-336.

[64] D. A. J. Rand, R. Woods, Journal of Electroanalytical Chemistry and Interfacial Electrochemistry 44 (1973) 83-89.

[65] A. T. Hubbard, Heterogeneous Chem. Rev. 1 (1994) 3.

[66] Y.-G. Kim, J. E. Soto, X. Chen, Y.-S. Park, M. P. Soriaga, J Electroanal Chem 554-555 (2003) 167-174.

[67] J. Inukai, M. Wakisaka, M. Yamagishi, K. Itaya, Langmuir 20 (2004) 7507-7511.

[68] Y.-G. Kim, J. H. Baricuatro, M. P. Soriaga, Langmuir 22 (2006) 10762-10765.

[69] Y.-G. Kim, S.-L. Yau, K. Itaya, Langmuir 15 (1999) 7810-7815.

[70] W.-B. Cai, L.-J. Wan, H. Noda, Y. Hibino, K. Ataka, M. Osawa, Langmuir 14 (1998) 6992-6998.

[71] L.-J. Wan, K. Itaya, Langmuir 13 (1997) 7173-7179.

[72] A. T. Hubbard, M. P. Soriaga, J. L. Stickney, J. H. White, J Electrochem Soc 130 (1983) C118-C119.

[73] E. Berliner, J Am Chem Soc 68 (1946) 49-51.

[74] J. L. Stickney, M. P. Soriaga, A. T. Hubbard, S. E. Anderson, J Electroanal Chem 125 (1981) 73-88.

[75] M. P. Soriaga, J. H. White, D. Song, V. K. F. Chia, P. O. Arrhenius, A. T. Hubbard, Inorg Chem 24 (1985) 73-79.

[76] J. E. Soto, Y. G. Kim, X. Chen, Y. S. Park, M. P. Soriaga, J Electroanal Chem 500 (2001) 374-378.

[77] Y. G. Kim, M. P. Soriaga, Phys Chem Chem Phys 3 (2001) 3303-3306.

[78] M. E. Bothwell, M. P. Soriaga, J Electroanal Chem 260 (1989) 193-199.

[79] D. Song, M. P. Soriaga, A. T. Hubbard, J Electroanal Chem 193 (1985) 255-264.

[80] G. Andreasen, M. E. Vela, R. C. Salvarezza, A. J. Arvia, Langmuir 13 (1997) 6814-6819.

[81] B. G. Bravo, S. L. Michelhaugh, T. Mebrahtu, M. P. Soriaga, Electrochim Acta 33 (1988) 1507-1511.

[82] T. Mebrahtu, M. E. Bothwell, J. E. Harris, G. J. Cali, M. P. Soriaga, Journal of Electroanalytical Chemistry and Interfacial Electrochemistry 300 (1991) 487-498.

[83] T. Mebrahtu, G. M. Berry, B. G. Bravo, S. L. Michelhaugh, M. P. Soriaga, Langmuir 4 (1988) 1147-1151.

[84] B. G. Bravo, S. L. Michelhaugh, M. P. Soriaga, Langmuir 5 (1989) 1092-1095.

[85] J. E. Soto, D. Li, J. Sanabria-Chinchilla, X. Chen, M. P. Soriaga, J Mol Struct 890 (2008) 298-302.

[86] A. S. Duwez, L. M. Yu, J. Riga, J. Delhalle, J. J. Pireaux, Langmuir 16 (2000) 6569-6576.

[87] Y.-T. Tao, C.-C. Wu, J.-Y. Eu, W.-L. Lin, K.-C. Wu, C.-h. Chen, Langmuir 13 (1997) 4018-4023.

[88] C. E. D. Chidsey, C. R. Bertozzi, T. M. Putvinski, A. M. Mujsce, J Am Chem Soc 112 (1990) 4301-4306.

VITA

Name:	Juan Cruz Jr.
Address:	Department of Chemistry, Texas A&M University 3255 TAMU College Station, TX 77842-3255
Email Address:	cruzj1903@netscape.net
Education:	B.S., Chemistry, University of Texas at El Paso, 1994 M.S., Chemistry, University of Texas at San Antonio, 2001